nature neuroscience

A supercritical density of Na^+ channels ensures fast signaling in GABAergic interneuron axons

Hua Hu & Peter Jonas

Fast-spiking, parvalbumin-expressing GABAergic interneurons, a large proportion of which are basket cells (BCs), have a key role in feedforward and feedback inhibition, gamma oscillations and complex information processing. For these functions, fast propagation of action potentials (APs) from the soma to the presynaptic terminals is important. However, the functional properties of interneuron axons remain elusive. We examined interneuron axons by confocally targeted subcellular patch-clamp recording in rat hippocampal slices. APs were initiated in the proximal axon ~20 μm from the soma and propagated to the distal axon with high reliability and speed. Subcellular mapping revealed a stepwise increase of Na^+ conductance density from the soma to the proximal axon, followed by a further gradual increase in the distal axon. Active cable modeling and experiments with partial channel block revealed that low axonal Na^+ conductance density was sufficient for reliability, but high Na^+ density was necessary for both speed of propagation and fast-spiking AP phenotype. Our results suggest that a supercritical density of Na^+ channels compensates for the morphological properties of interneuron axons (small segmental diameter, extensive branching and high bouton density), ensuring fast AP propagation and high-frequency repetitive firing.

Fast-spiking, parvalbumin-expressing GABAergic interneurons, a large fraction of which are BCs, have a key role in the function of neuronal networks. These interneurons mediate fast feedforward and feedback inhibition[1–3], generate network oscillations in the gamma frequency range[4–6], and contribute to complex information processing in neuronal networks, such as pattern separation[7]. For all of these functions, the speed and reliability of signaling of GABAergic interneurons is critically important. In essence, BCs need to convert an excitatory input signal into an inhibitory output signal in a millisecond or less[8]. Furthermore, BCs need to reliably distribute this output signal onto a large number of target cells[9]. However, the subcellular mechanisms underlying speed and reliability in this important type of GABAergic interneuron remain largely unclear.

The axon is a critical site for input-output conversion because it mediates AP initiation, AP propagation and transmitter release[10,11]. Two major mechanisms are generally thought to promote rapid signal propagation in axons in the mammalian nervous system: large axon diameter and myelination[10]. However, BC axons have a small diameter, branch extensively and give rise to numerous en-passant boutons[9]. Thus, enlargement of axon diameter may not be possible because of spatial constraints and myelination is precluded by the spatially overlapping functions of AP propagation and transmitter release. In a schematic ball-and-stick model, both axon collaterals and en-passant presynaptic terminals markedly decrease the speed and reliability of AP propagation (**Supplementary Fig. 1**). Thus, the cable structure of interneuron axons appears to be highly unfavorable for rapid and reliable AP propagation.

How is fast and reliable signaling in BC axons achieved in the presence of these morphological challenges? To address this question, we developed confocally targeted subcellular patch-clamp techniques that allow us to directly record from interneuron axons. Our results suggest that the Na^+ conductance in BC axons is above the critical minimum required to ensure reliability and that this supercritical density is important to ensure both the speed of AP propagation and the fast-spiking AP phenotype (also see H. Hu and P. Jonas, *Soc. Neurosci. Abstr.* **238.06**, 2012).

RESULTS

To directly examine the functional properties of interneuron axons, we performed confocally targeted subcellular patch-clamp recordings from fast-spiking, parvalbumin-expressing GABAergic interneurons in acute hippocampal slices[12] (**Fig. 1**). Axonal recordings were established in three steps. First, a somatic recording was obtained with a patch pipette containing Alexa Fluor 488. Second, the axon was visualized using fast confocal imaging after ~30 min of filling time. Finally, recordings were made from either axon shafts (27 simultaneous axon-soma recordings) or small spherical axon expansions (87 simultaneous axon-soma recordings), which probably represent axon 'blebs'[13]. Axonal recordings were readily obtained, consistent with the absence of myelination in BC axons. Lack of myelin was confirmed by the absence of double immunolabeling for myelin basic protein (MBP) and parvalbumin in the dentate gyrus granule cell layer[14] (**Fig. 1e** and **Supplementary Fig. 2**). Confocally targeted subcellular patch-clamp recording from BCs allowed us to measure absolute voltage changes in the axon with microsecond temporal resolution at defined locations up to 418 μm from the soma, covering a major part of the axonal arborization of these GABAergic interneurons[9].

IST Austria, Klosterneuburg, Austria. Correspondence should be addressed to H.H. (hua.hu@ist.ac.at) or P.J. (peter.jonas@ist.ac.at).

Received 17 January; accepted 13 February; published online 23 March 2014; doi:10.1038/nn.3678

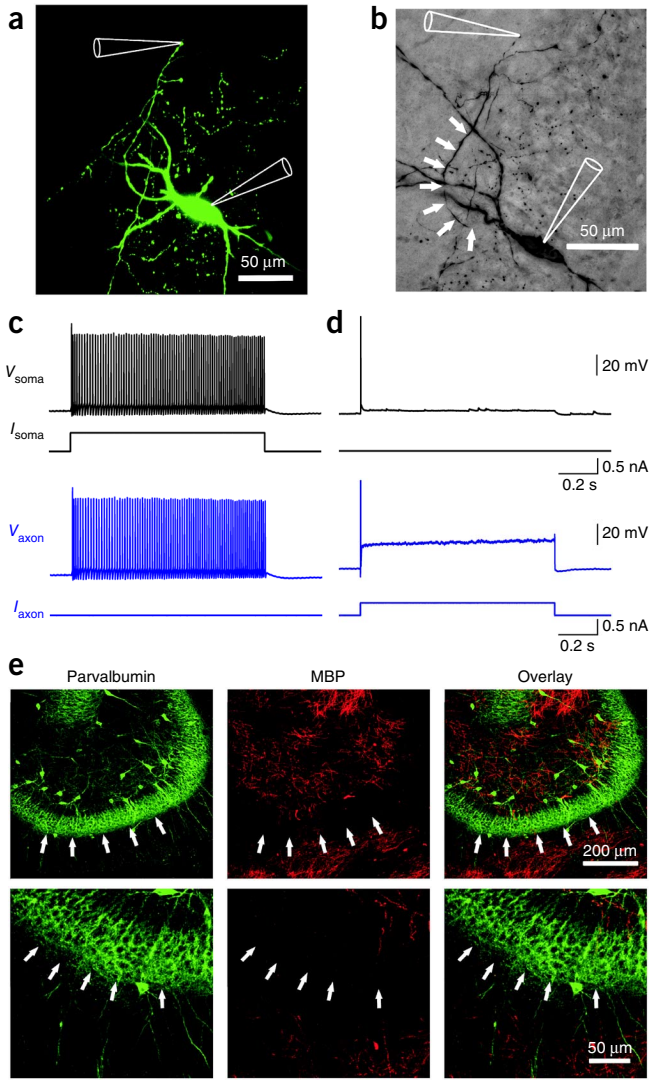

Figure 1 Confocally targeted subcellular patch-clamp recording from axons of hippocampal fast-spiking, parvalbumin-expressing GABAergic interneurons. (**a**) Confocal image of a BC in the dentate gyrus filled with Alexa Fluor 488 during the experiment. Confocal stack maximum projection. (**b**) Same cell filled with biocytin during recording and labeled with 3,3′-diaminobenzidine as chromogen. White arrows indicate the axon trajectory. In **a** and **b**, recording pipettes are illustrated schematically. (**c**,**d**) Train of APs evoked by a 1-s depolarizing current pulse applied at the soma (**c**) and the axon (at 177 µm; **d**). Black traces, somatic voltage and corresponding current. Blue traces, axonal voltage and corresponding current. Data in **a**–**d** are from the same cell. (**e**) Double immunolabeling for parvalbumin (a selective marker of fast-spiking GABAergic interneurons) and MBP (a specific marker of myelination). Left, parvalbumin; center, MBP; right, overlay. Note the absence of colocalization between the two markers in the granule cell layer, suggesting that BC axons are largely unmyelinated. Experiments were repeated on five rats, giving consistent results. White arrows indicate the outer border of the granule cell layer. Lower micrographs are expanded versions of upper images.

Initiation and propagation of APs in BC axons

To determine the site of AP initiation and the characteristics of propagation, we made simultaneous recordings from the soma and the axon at various distances (**Fig. 2**). APs were evoked by somatic current injection and the latency between somatic and axonal APs was measured using the time points corresponding to half-maximal amplitude in the AP rising phase. For proximal axonal recording sites, the axonal AP preceded the somatic waveform, suggesting that the recording electrode was close to the site of AP initiation (**Fig. 2a**). For distal axonal recording sites, the somatic AP preceded the axonal signal, suggesting that the recording site was distal to the AP initiation site (**Fig. 2b**). To quantitatively localize the exact site of AP initiation during somatic current injection, we plotted the latency between somatic and axonal APs against the distance between the recording sites (**Fig. 2c**). Notably, the latency-distance relation showed a sharp minimum at ~20 µm from the soma, indicating a proximal site of AP initiation in these GABAergic interneurons (62 simultaneous axon-soma recordings; **Fig. 2c**). The latency-distance relation for the 20th AP in a high-frequency train showed a very similar minimum (**Fig. 2c**), indicating that the location of the AP initiation site was constant during high-frequency firing. Thus, APs were robustly initiated in the axon at a proximal site. This situation is different from that in glutamatergic pyramidal neurons, where the AP initiation site is more remote[15–19].

To probe the reliability of AP propagation, we applied high-frequency trains of brief current pulses at the soma (120 APs at 100 Hz; **Fig. 2d–f**). Reliability was quantified as either the instantaneous AP frequency in the axon versus time during the train in a given cell (**Fig. 2e**) or as the ratio of somatic and axonal AP number versus distance in the cell population (**Fig. 2f**). The instantaneous AP frequency in the BC axon was identical to the corresponding somatic AP frequency, and the ratio of axonal to somatic AP number was close to 1 (28 simultaneous axon-soma recordings). Identical results were obtained for high-frequency trains of APs evoked by 1-s depolarizing current pulses at the soma (86.4 ± 1.9 Hz, 92 simultaneous axon-soma recordings at distances of up to 418 µm from the soma). Thus, APs propagate from the initiation site into the distal BC axon with high reliability.

Finally, we quantified the velocity of AP propagation, fitting the latency-distance relation with a bilinear function with sigmoidal transition (**Fig. 2c**). On average, the velocity of orthodromic propagation was 0.52 m s^{-1} for the first AP and 0.49 m s^{-1} for the 20th AP in a high-frequency train. Similar results were obtained at near-physiological temperature (30–33 °C); under these conditions the orthodromic propagation velocity was 1.45 m s^{-1} for the first AP and 1.42 m s^{-1} for the 20th AP in a high-frequency train (19 simultaneous axon-soma recordings; **Supplementary Fig. 3**). Thus, the conduction velocity is higher than that of unmyelinated axons of glutamatergic principal neurons under similar conditions[20,21].

Mechanisms of AP initiation and propagation

What are the mechanisms underlying the robust AP initiation in the proximal part and the reliable and fast propagation into distal parts of the interneuron axon? In pyramidal neurons, a high density of Na^+ channels in the axon initial segment is thought to convey AP initiation at a proximal site[22,23]. To test whether the Na^+ channel distribution was similar in fast-spiking GABAergic interneurons, we measured Na^+ channel density in axons using outside-out patches isolated at various distances from the soma (**Fig. 3**). Notably, depolarizing voltage pulses evoked a large transient Na^+ current in membrane patches isolated from both proximal and distal axonal sites, in marked contrast with the small current observed in somatic patches (**Fig. 3a**). To convert Na^+ current amplitude into Na^+ conductance density, we further determined the patch area by capacitance measurements (**Supplementary Fig. 4**). Plotting the maximal Na^+ conductance density $\overline{g}_{Na}$ against distance revealed a stepwise increase from the soma to the proximal

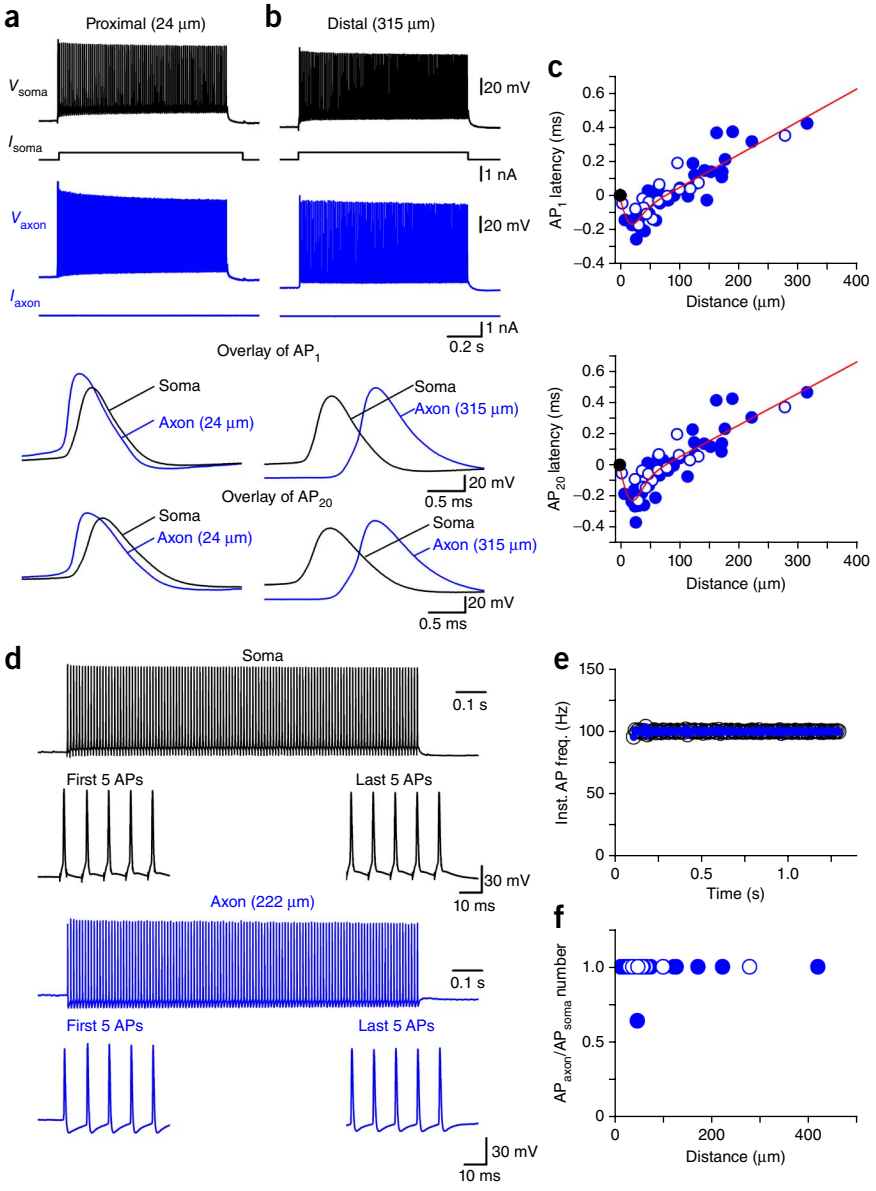

Figure 2 Proximal initiation and fast, reliable propagation of APs in interneuron axons. (**a**) Simultaneous recording from the soma and the axon of a fast-spiking, parvalbumin-expressing BC during a long somatic current pulse. Black traces, somatic voltage and corresponding current; blue traces, axonal voltage and corresponding current. The axonal recording site was located 24 µm from the soma. Bottom traces show expanded views of the first (AP_1) and the 20th (AP_{20}) in the high-frequency train. (**b**) Another simultaneous recording from the soma and the axon, in which the axonal recording site was located 315 µm from the soma. (**c**) Plot of latency between somatic and axonal AP against distance of the axonal recording site from the soma for the first AP (top) and the 20th AP (bottom). Data from 62 axon-soma recordings. Data were fit with a bilinear function (continuous red line), giving a minimal latency at 20 and 22 µm and a propagation velocity of 0.52 m s^{-1} and 0.49 m s^{-1} for the first and the 20th AP, respectively. Filled circles represent recordings from axon varicosities and open circles represent recordings from axon shafts. (**d**) Simultaneous recording from the soma and the axon of a BC during a high-frequency train of short somatic current pulses (120 stimuli at 100 Hz; 3 ms, 1 nA). Black, somatic voltage; blue, axonal voltage. The axonal recording site was located 222 µm from the soma. (**e**) Plot of instantaneous somatic and axonal AP frequency during the stimulation train (same cell as shown in **d**). (**f**) Plot of ratio of number of APs in the axon over number of APs in the soma, plotted against distance of the axonal recording site. Data from 28 simultaneous axon-soma recordings.

axon, followed by a further gradual increase in the distal axon (**Fig. 3b**). On average, $\overline{g_{Na}}$ was 31.9 ± 3.7 pS µm^{-2} at the soma, 310.7 ± 32.7 pS µm^{-2} in the proximal axon, and 574.3 ± 120.8 pS µm^{-2} in the distal axon ($P < 0.05$; **Fig. 3c** and **Supplementary Table 1**). Thus, the Na^+ conductance in BC axons was comparable to that of highly excitable invertebrate axons[24,25].

To convert conductance density into channel density, we performed a nonstationary fluctuation analysis of Na^+ currents in outside-out patches isolated from BC axons[26] (**Fig. 3d–f**). This analysis revealed a single-channel conductance of 12.5 ± 1.0 pS and a maximal channel open probability of 0.66 ± 0.05 (five axon patches, test pulse amplitude 0 mV). Based on these values, we estimate that the Na^+ channel density was 2.6 channels µm^{-2} in the soma, 25.0 channels µm^{-2} in the proximal axon, and 46.1 channels µm^{-2} in the distal axon (**Fig. 3g**). To quantitatively assess the Na^+ peak conductance distribution, we compared a linear model, a step function and a combined step-linear function. The combined step-linear function fit the data significantly better than the other models ($P < 0.002$), and all three functions fit the data significantly better than Gaussian functions with maximal density in the first 100 µm ($P < 0.01$). Thus, the Na^+ channel distribution in BC axons markedly differs from that in principal neuron axons, where Na^+ channels are concentrated in the axon initial segment[22,27–31].

Further analysis of gating kinetics and voltage-dependence of activation and inactivation revealed that Na^+ channels in BC axons differed from somatic channels in their functional properties. First, the gating kinetics was faster for axonal than for somatic Na^+ channels (**Supplementary Fig. 5**). The activation time constant was 64 ± 6 µs in the axon versus 122 ± 34 µs in the soma ($P > 0.2$, four axonal and nine somatic patches) and the inactivation time constant was 303 ± 21 µs in the axon and 728 ± 98 µs in the soma ($P < 0.01$, 11 axonal and nine somatic patches, respectively, test pulse amplitude = 0 mV). Thus, the inactivation time constant was 2.4-fold faster for axonal than for somatic Na^+ channels. Furthermore, the midpoint potential of the activation curve of axonal channels was 10.9 mV more negative than that of somatic channels, whereas differences in the midpoint potential of the inactivation curves were less prominent ($P < 0.01$; **Supplementary Fig. 6** and **Supplementary Table 1**). In conclusion, our results suggest that the functional properties of Na^+ channels in BC axons are specialized, in particular with respect to rapid inactivation kinetics. Rapid inactivation of axonal

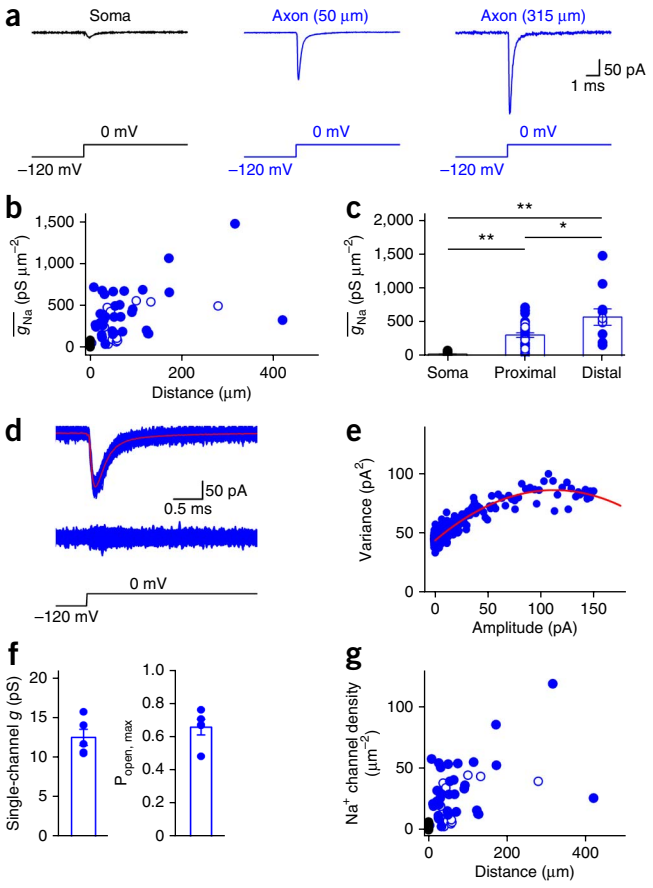

Figure 3 A high Na^+ channel density in interneuron axons. (**a**) Na^+ current in an outside-out patch in the soma, proximal axon (50 µm) and distal axon (315 µm from the soma). Na^+ currents were evoked by a sequence of a prepulse to −120 mV followed by a test pulse to 0 mV (bottom). Black trace, somatic patch; blue traces, axonal patches. (**b**) Summary plot of Na^+ conductance density ($\overline{g_{Na}}$) against distance from the soma. Data from 48 axonal recordings and 24 somatic recordings. (**c**) Summary bar graph showing $\overline{g_{Na}}$ in the soma (24 patches), proximal axon (<100 µm, 37 patches) and distal axon (≥100 µm, 11 patches). Bars indicate mean ± s.e.m., circles represent data from individual experiments. *$0.01 \le P < 0.05$, **$P < 0.01$. (**d**) Top, overlay of 300 axonal Na^+ current traces, superimposed with the average (red). Center, superimposition of the difference of individual current traces from the mean. Bottom, voltage-clamp protocol for evoking Na^+ current. (**e**) Plot of variance versus mean from the experiment shown in **d**. Red curve represents a parabolic function fit to the data points. (**f**) Summary bar graph of single-channel conductance and maximal open probability of Na^+ channels (both at 0 mV). Bars indicate mean ± s.e.m., circles represent data from individual experiments. (**g**) Summary plot of Na^+ channel density against distance from the soma. In **b**, **c** and **g**, black symbols represent somatic patches, blue symbols represent axonal patches, filled circles represent recordings from axon varicosities and open circles represent recordings from axon shafts.

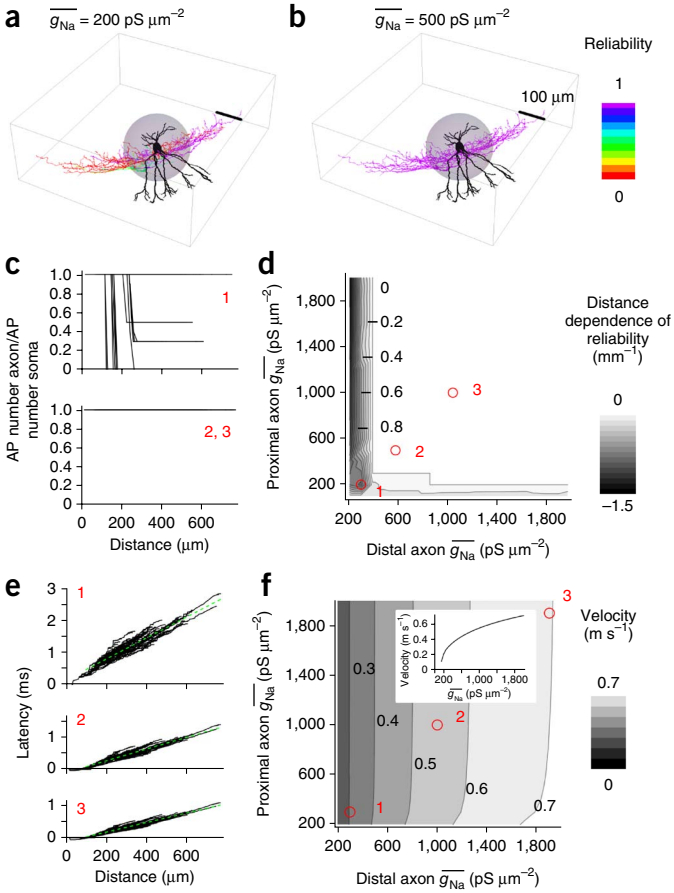

Figure 4 Dependence of reliability and velocity of AP propagation on axonal Na^+ conductance density in an active BC model. (**a**,**b**) Plot of reliability of AP propagation, shown as color coding of the surface of the reconstructed neuron for $\overline{g_{Na}}$ = 200 pS µm^{-2} (**a**) and 500 pS µm^{-2} (**b**); proximal and distal $\overline{g_{Na}}$ were changed in parallel. Color scale bar indicates the reliability of propagation in the axon (inset, right); dendrites are depicted in black to indicate the lack of active AP propagation. Gray sphere represents the proximal region of the axon. (**c**,**d**) AP propagation reliability-distance plots (**c**) and contour plot of the average slope of the reliability-distance relation as a function of proximal and distal $\overline{g_{Na}}$ (**d**). Red circles and numbers in **d** indicate the correspondence with the graphs shown in **c**. Numbers right-adjacent to contour lines in **d** indicate distance dependence of AP propagation reliability (in mm^{-1}, values in the range ±0.02 are represented as 0, see gray scale bar on the right). In **a**–**d**, 100-Hz trains of ten brief stimuli were applied to the soma and the number of successfully propagated APs in the axon was plotted against distance. (**e**,**f**) Latency-distance plots (**e**) and contour plot of AP propagation velocity as a function of proximal and distal $\overline{g_{Na}}$ (**f**). Dashed green lines in **e** indicate the results of linear regression for distances >100 µm. Numbers right-adjacent to contour lines in **f** indicate AP propagation velocity (in m s^{-1}; see gray scale bar on the right). Red circles and numbers in **f** indicate the correspondence with the graphs shown in **e**. Inset in **f** shows one-dimensional representation for simultaneous changes in proximal and distal $\overline{g_{Na}}$. In **e** and **f**, single brief stimuli were used to evoke APs. All simulations were performed on cell 2 from ref. 9.

Na^+ channels may increase the energetic efficiency of the AP in GABAergic interneuron axons[32,33].

Na^+ channel density determines AP propagation speed

To quantitatively examine the relation between Na^+ conductance density and AP propagation, we developed an active, morphologically realistic cable model of a fast-spiking GABAergic interneuron (**Fig. 4**). Voltage-gated Na^+ and K^+ channels represented by a Hodgkin-Huxley–type model[34,35] were incorporated into a detailed cable conductor model of a hippocampal BC (including soma, dendrites, and the entire axonal arborization[9]). The Na^+ conductance in the proximal and distal axon was varied over a 20-fold range. We first examined how Na^+ conductance affected the reliability of AP propagation[10,11] (**Fig. 4a–d**). A 100-Hz train of ten APs was evoked by somatic current injection, reliability was computed for each axonal distance as the ratio of axonal over somatic AP number (**Fig. 4c**), and the global

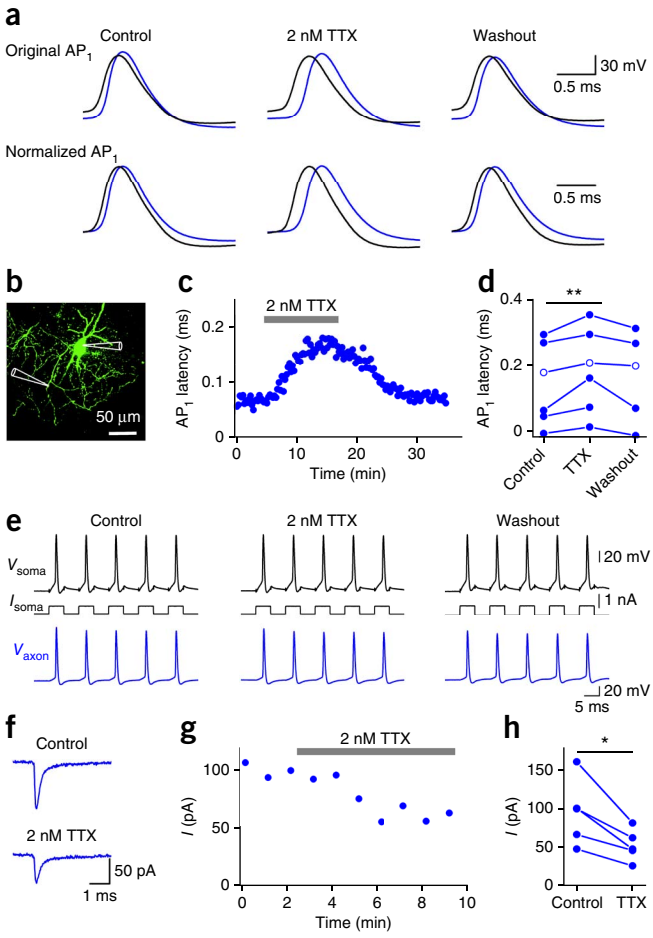

Figure 5 A supercritical Na^+ channel density in the axon ensures fast AP propagation. (**a**) Simultaneous axon-soma recordings in control conditions, in the presence of 2 nM TTX, and after washout (first AP, AP_1). Upper traces are displayed at absolute voltage scale, lower traces are shown normalized to the same peak amplitude to facilitate comparison of the rising phase. (**b**) Confocal stack maximum projection of a recorded BC. Recording pipettes are illustrated schematically. (**c**) Plot of latency between somatic and axonal AP against experimental time during application of 2 nM TTX (horizontal bar). (**d**) Summary graph of the effects of 2 nM TTX on latency between somatic and axonal AP. Data from six simultaneous axon-soma recordings at distances of 91 to 222 µm. Data from the same experiment were connected by lines. Open circles represent data from the cell shown in **Supplementary Figure 10**. (**e**) Effects of 2 nM TTX on reliability of AP propagation during a high-frequency train (five stimuli at 100 Hz; 5 ms, 0.7 nA). Data in **a**–**c** and **e** were obtained from the same experiment (axonal recording site was 100 µm from the soma). (**f**) Na^+ current recorded from an outside-out patch isolated from the axon 66 µm from the soma before and after bath application of 2 nM TTX. Na^+ currents were evoked by a sequence of a prepulse to −120 mV followed by a test pulse to 0 mV. (**g**) Plot of Na^+ current peak amplitude against experimental time during application of 2 nM TTX (horizontal bar) from the experiment shown in **f**. Each data point represents the average of six consecutive peak current values. (**h**) Summary graph of the effects of 2 nM TTX on Na^+ peak current. Data from five axonal outside-out patches. Data from the same experiment were connected by lines. In **d** and **h**, $*0.01 \le P < 0.05$, $**P < 0.01$.

propagation characteristics were quantified as the slope of the reliability-distance curve (**Fig. 4d**). In the model, AP propagation was absolutely reliable above a critical value of $\overline{g_{Na}} > 200$ pS µm^{-2} in the proximal and distal axon. The experimentally determined $\overline{g_{Na}}$ was ~1.5-fold higher than the critical value (defined based on reliability of AP propagation) in the proximal axon and ~2.8-times higher in the distal axon, indicating that Na^+ channels in BC axons were expressed at 'supercritical' density above the minimum required to ensure reliable AP propagation. Next, we tested how Na^+ conductance affected the velocity of AP propagation (**Fig. 4e**,**f**). Increasing the Na^+ conductance density above the critical value markedly increased the velocity of AP propagation. When $\overline{g_{Na}}$ in both the proximal and distal axon was increased from 200 to 2,000 pS µm^{-2}, the AP conduction velocity increased 3.27-fold (**Fig. 4f**). We obtained similar results in five other fully reconstructed cells (**Supplementary Fig. 7**)[9]. Furthermore, similar results were obtained after increasing or decreasing the axon diameter by a factor of 1.5. Although increasing the axon diameter increased propagation velocity, whereas decreasing axon diameter decreased it, the dependence of velocity on $\overline{g_{Na}}$ qualitatively remained the same (**Supplementary Fig. 8a**,**b**). Thus, our conclusions were independent of the details of morphological properties of the BC axon. Finally, changing the gating kinetics of Na^+ channel inactivation and K^+ channel activation by a factor corresponding to a temperature change of 5 °C had only minimal effects on reliability and speed of AP propagation (**Supplementary Fig. 8c**,**d**). Taken together, these results suggest that a low Na^+ channel density in the BC axon is sufficient for reliability, whereas a high density is necessary for fast AP propagation.

To experimentally test this hypothesis, we measured AP latencies between somatic and axonal sites in the presence of a low concentration of the Na^+ channel blocker tetrodotoxin (TTX; **Fig. 5**). Bath application of 2 nM TTX in simultaneous axon-soma recordings significantly affected latency. On average, the latency of the first AP in a high-frequency train increased to 131% of the control value (six simultaneous axon-soma recordings at distances between 91 to 222 µm, $P < 0.01$; **Fig. 5a–d**). In contrast, the reliability of AP propagation during high-frequency trains in the same recordings was maintained (**Fig. 5e**). Consistent with these results, bath application of 2 nM TTX also increased the latency of unitary inhibitory postsynaptic currents (IPSCs) in synaptically connected BC–granule cell pairs (**Supplementary Fig. 9**). Under comparable conditions, bath application of 2 nM TTX blocked 43.1 ± 3.9% of Na^+ current in axonal outside-out patches (five axon patches, $P < 0.05$; **Fig. 5f–h**). These results are consistent with the predictions of the active interneuron models (**Supplementary Fig. 10**), providing further evidence that a supercritical Na^+ channel density in the BC axon is necessary for fast AP propagation.

Na^+ channel density contributes to AP phenotype

Our results indicate that axonal Na^+ channel density affects reliability and velocity of AP propagation. Does it also affect the AP phenotype itself, such as the ability of BCs to generate high-frequency trains of APs[36,37]? To test whether the Na^+ channel conductance density affects the fast-spiking AP generation, we again used a combined computational-experimental approach (**Fig. 6**). We first computed the dependence of maximal AP frequency during long current pulses on $\overline{g_{Na}}$ in the proximal and distal axon (**Fig. 6a**,**b**). Axonal Na^+ conductance density markedly affected the maximal AP frequency during long current pulses. Notably, whereas the speed and reliability of AP propagation were primarily determined by $\overline{g_{Na}}$ in the distal axon (**Fig. 4d**,**f**), maximal firing frequency was largely controlled by $\overline{g_{Na}}$ in the proximal axon (**Fig. 6b**). To experimentally test the hypothesis that a high axonal Na^+ channel density contributes to the fast-spiking AP phenotype, we measured AP frequency during long current pulses before and after bath application of a low concentration

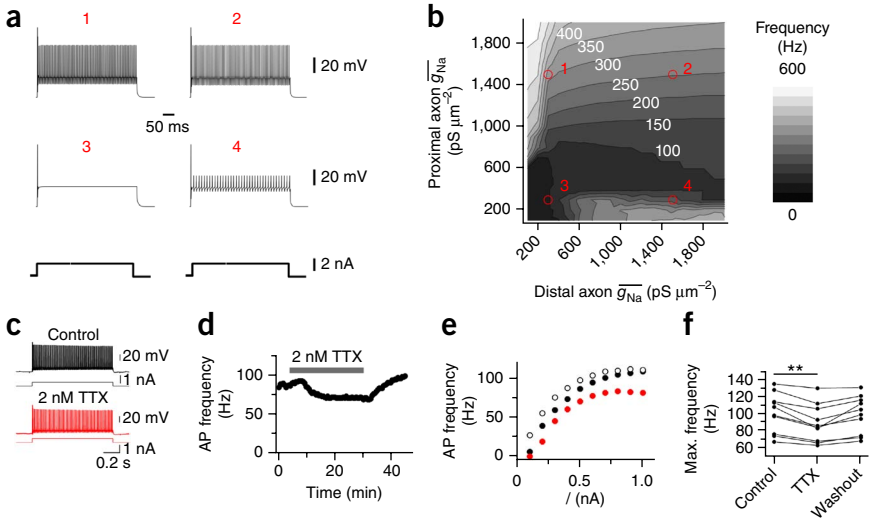

Figure 6 A supercritical Na^+ channel density contributes to the fast-spiking AP phenotype. (**a**,**b**) Effects of Na^+ conductance density on fast-spiking AP phenotype in a BC model. Example traces (**a**) and contour plot (**b**) of maximal AP frequency as a function of proximal and distal $\overline{g_{Na}}$. Red circles and numbers in **b** indicate the correspondence with the graphs shown in **a**. White numbers right-adjacent to contour lines in **b** indicate maximal AP frequency (in Hz; see gray scale bar on the right). APs were evoked by 500-ms current pulses (0.5–5 nA, 0.5 nA steps; 2.5 nA in **a**). (**c**–**f**) Effects of 2 nM TTX on fast-spiking AP phenotype in experimental conditions. (**c**) Train of APs evoked by long current pulses under control conditions (top, black trace) and in the presence of 2 nM TTX (bottom, red trace). (**d**) Plot of AP frequency in spike trains evoked by a 1-s depolarizing current pulse against experimental time during application of 2 nM TTX (horizontal bar). 500-pA current pulses were applied throughout. Data in **c**–**e** are from the same cell. (**e**) Frequency-current relation in control conditions (black filled circles), in the presence of 2 nM TTX (red circles), and after washout (black open circles). Note that 2 nM TTX slightly, but reversibly, reduced the maximal AP frequency. (**f**) Summary graph of the effects of 2 nM TTX on maximal AP frequency. Data are from ten BCs. Data from the same experiment were connected by lines. $^{**}P < 0.01$.

of TTX. In these experiments, 2 nM TTX significantly and reversibly reduced the maximal AP frequency (ten BC somatic recordings, $P < 0.01$; **Fig. 6c–f**). These results suggest that a supercritical Na^+ channel density in the BC axon is necessary for the fast-spiking AP phenotype.

DISCUSSION

Our results reveal several unexpected functional properties of axons of fast-spiking, parvalbumin-expressing GABAergic interneurons. First, APs were initiated in the proximal axon very close to the soma, and propagated to the distal axon with high reliability and speed. Second, BCs showed a unique Na^+ channel distribution profile, with a stepwise increase of Na^+ conductance density from the soma to the proximal axon, followed by a further gradual increase in the distal axon. Third, our results suggest that the Na^+ conductance in BC axons exceeded the critical minimum required to ensure reliability and that this high density was necessary to ensure both the speed of AP propagation and the fast-spiking AP phenotype. Thus, a supercritical density of Na^+ channels compensates for the morphological properties of interneuron axons (small segmental diameter, extensive branching and high bouton density), ensuring rapid signaling in BCs.

Specific properties of AP initiation and propagation

The rules of AP initiation and propagation in BCs differ from those in pyramidal neurons in multiple ways. First, APs in BCs are robustly initiated at a proximal site, only ~20 µm from the soma. In contrast, in cortical pyramidal neurons, the initiation site is more remote[16,17], sometimes even beyond the axon initial segment[15]. Second, APs in BCs propagate with almost absolute reliability, even during high-frequency trains. In contrast, in pyramidal neurons, propagation appears to be less reliable[38–40]. Finally, we found that APs propagate in the BC axon with high speed. We estimate that the propagation velocity is ~0.5 m s^{-1} at ~22 °C and ~1.5 m s^{-1} at near-physiological temperature. In contrast, AP propagation in nonmyelinated collaterals of principal neurons is slower (0.36 m s^{-1} in CA3 pyramidal neurons[20], 0.24 m s^{-1} in dentate gyrus granule cells[21], all values at ~22 °C).

Unique Na^+ channel distribution profile

Our results reveal a unique spatial profile of Na^+ channel distribution in BCs. Na^+ channel density exhibits a ~10-fold stepwise increase from the soma to the proximal axon, followed by a further gradual increase in the distal axon. In contrast, Na^+ channel density is very low in the dendrites[12]. This channel distribution is different from that in cortical principal neurons, where Na^+ channel density shows a peak in the axon initial segment, but is also substantial in the dendrites[22,27–30]. Thus, unlike many other cell types, BCs show a high degree of polarity, with a nonexcitable input region connected to a highly excitable output region.

The steep gradient in Na^+ channel density between the soma and the axon initial segment appears to be sufficient to define the proximal initiation site; an absolute maximum of Na^+ channel density in the initial segment is not required[18,29,41]. In addition, the left-shifted activation curve of axonal Na^+ channels may contribute to proximal initiation[42], amplifying the gradient of available channels into a larger gradient of open channels. Furthermore, the high Na^+ channel density in the distal axon is important for ensuring both the reliability and speed of AP propagation. However, the two factors are differentially sensitive to Na^+ conductance density. A low (critical) axonal Na^+ conductance density was sufficient for reliability, whereas a high (supercritical) density was necessary to guarantee speed.

Effects of structural factors

Two structural factors are generally thought to accelerate AP propagation in axons[10]. One mechanism, used in invertebrates, is the increase of axon diameter, resulting in propagation velocities of up to ~20 m s^{-1} (ref. 34). Another mechanism is the formation of a myelin sheath, generating saltatory conduction[43]. However, BC axons do not exploit these strategies. Average axon diameter is in the submicrometer range[9], and myelination is largely absent, as indicated by the lack of MBP immunoreactivity (Online Methods). Furthermore, BC axons show several structural properties that are expected to slow down AP propagation, particularly a large number of axon collaterals and a high density of en-passant boutons[9]. The negative influence of both axon collaterals and boutons is shown in our schematic ball-and-stick model (**Supplementary Fig. 1**), and the effect of en-passant boutons

is further exemplified in hippocampal mossy fiber axons, in which the pearl-chain arrangement of large presynaptic terminals slows propagation[44]. We found that the supercritical Na^+ channel density in the BC axon compensates for these factors. In addition, structural details may be important for AP propagation. First, branching of BC axons was often asymmetric, leading to geometric ratios close to 1 (**Supplementary Fig. 7**)[9]. Second, the majority of BC en-passant boutons had a diameter of <2 µm, which is much smaller than that of mossy fiber terminals. Consequently, the negative effects of structural determinants on propagation velocity will be minimized, and compensation by the high axonal Na^+ channel density will be more efficient.

Consequences for the fast-spiking AP phenotype

BCs generate APs at high frequency both under *in vitro* and *in vivo* conditions[4,45]. Previous studies demonstrated that the expression of voltage-gated K^+ channels of the Kv3 subtype has a key role in the fast-spiking AP phenotype[36,46]. However, we found that the high axonal Na^+ channel density is also critical. High Na^+ channel density may have direct consequences, increasing the number of available Na^+ channels during an AP train[37]. In parallel, high Na^+ channel density may have several indirect effects. For example, it will increase the amplitude of the AP overshoot, resulting in more efficient activation of Kv3 channels. This, in turn, will promote recovery of Na^+ channels from inactivation. Our simulations suggest that the Na^+ conductance in the proximal axon is more relevant for the fast-spiking phenotype than that in the distal axon (**Fig. 6b**). In contrast, distal Na^+ conductance was more important for AP propagation velocity (**Fig. 4f**). Thus, although a high Na^+ conductance is required for both fast propagation and high-frequency firing pattern, the responsible channels are located in different axonal subdomains.

Implications for brain energetics

Because of their high AP frequency under *in vitro* and *in vivo* conditions[4,45], BCs are expected to make a major contribution to the energy budget of the brain. From the perspective of energetics, the expression of a high density of Na^+ channels in the axon may be disadvantageous. Both the synthesis of Na^+ channel proteins and the reestablishment of ion gradients after an AP via the Na^+/K^+ ATPase require ATP, with metabolic costs roughly proportional to channel number. This suggests that the advantages of the supercritical Na^+ channel density (for example, fast signaling) may outweigh the disadvantages (high energy consumption). However, our results indicate that Na^+ channels in BC axons have specialized gating properties, particularly rapid inactivation. These differences in gating kinetics may be generated by different abundance of Na^+ channel alpha subunits (Nav1.1 versus 1.6) and/or beta subunits (β1, β2 or β4)[47]. Thus, the specific subunit composition of Na^+ channels in the BC axon will minimize Na^+ inflow during APs and reduce associated metabolic costs[32,33].

Implications for microcircuit and network function

Our findings suggest a likely picture of how fast-spiking, parvalbumin-expressing interneurons operate in the neuronal network. In combination, the absence of Na^+ channels and the presence of Kv3-type K^+ channels in the dendrites conveys sublinear integration properties to these cells and makes them particularly sensitive to distributed input[12]. In contrast, the high density of Na^+ channels in the axon conveys robust analog-digital conversion and rapid propagation of the digital signal. These cellular properties are expected to be critically important for the function of BCs, which mediate fast feedforward and feedback inhibition in hippocampal microcircuits[2,3]. It is well established that the time required for disynaptic inhibition in microcircuits can be as short as 1 ms (ref. 8). Our results identify fast axonal propagation of APs as a key factor underlying rapid disynaptic inhibition.

Finally, our findings may be relevant for the understanding of dynamic network activity. Fast-spiking, parvalbumin-expressing GABAergic interneurons are important for the generation of network oscillations in the gamma frequency range[4–6]. Establishing coherent oscillations in principal neuron–interneuron networks over distance is difficult, as axonal delays will disrupt the synchrony between spatially distributed cells[48–50]. Expression of Na^+ channels at a supercritical density in interneuron axons could extend the synchronization process over long distances, contributing to the generation of fast and coherent oscillatory reference signals for coding of information in memory circuits. Finally, our results may imply that the specific organization of excitability in interneuron axons could be altered in network diseases. Future work will be needed to address this possibility.

METHODS

Methods and any associated references are available in the online version of the paper.

Note: Any Supplementary Information and Source Data files are available in the online version of the paper.

ACKNOWLEDGMENTS

We thank D. Debanne, J. Guzmán and R. Shigemoto for critically reading previous versions of the manuscript. We also thank F. Marr and M. Duggan for technical assistance, A. Schlögl for programming, E. Kramberger and A. Solymosi for editorial support, and M. Hines and T. Carnevale for useful suggestions. P.J. was supported by the European Union (ERC advanced grant 268548) and the Fond zur Förderung der wissenschaftlichen Forschung (FWF grant P24909-B24).

AUTHOR CONTRIBUTIONS

H.H. performed experiments and analyzed the data. P.J. performed modeling and wrote the paper. Both authors jointly revised the paper.

COMPETING FINANCIAL INTERESTS

The authors declare no competing financial interests.

1. Freund, T.F. & Katona, I. Perisomatic inhibition. *Neuron* **56**, 33–42 (2007).
2. Buzsáki, G. & Eidelberg, E. Commissural projection to the dentate gyrus of the rat: evidence for feed-forward inhibition. *Brain Res.* **230**, 346–350 (1981).
3. Pouille, F. & Scanziani, M. Enforcement of temporal fidelity in pyramidal cells by somatic feed-forward inhibition. *Science* **293**, 1159–1163 (2001).
4. McBain, C.J. & Fisahn, A. Interneurons unbound. *Nat. Rev. Neurosci.* **2**, 11–23 (2001).
5. Bartos, M., Vida, I. & Jonas, P. Synaptic mechanisms of synchronized gamma oscillations in inhibitory interneuron networks. *Nat. Rev. Neurosci.* **8**, 45–56 (2007).
6. Cardin, J.A. *et al.* Driving fast-spiking cells induces gamma rhythm and controls sensory responses. *Nature* **459**, 663–667 (2009).
7. de Almeida, L., Idiart, M. & Lisman, J.E. A second function of gamma frequency oscillations: an *E*%-max winner-take-all mechanism selects which cells fire. *J. Neurosci.* **29**, 7497–7503 (2009).
8. Miles, R. Synaptic excitation of inhibitory cells by single CA3 hippocampal pyramidal cells of the guinea-pig *in vitro*. *J. Physiol. (Lond.)* **428**, 61–77 (1990).
9. Nörenberg, A., Hu, H., Vida, I., Bartos, M. & Jonas, P. Distinct nonuniform cable properties optimize rapid and efficient activation of fast-spiking GABAergic interneurons. *Proc. Natl. Acad. Sci. USA* **107**, 894–899 (2010).
10. Hille, B. *Ion Channels of Excitable Membrane* (Sinauer, Sunderland, Massachusetts, 2001).
11. Debanne, D., Campanac, E., Bialowas, A., Carlier, E. & Alcaraz, G. Axon physiology. *Physiol. Rev.* **91**, 555–602 (2011).
12. Hu, H., Martina, M. & Jonas, P. Dendritic mechanisms underlying rapid synaptic activation of fast-spiking hippocampal interneurons. *Science* **327**, 52–58 (2010).
13. Shu, Y., Hasenstaub, A., Duque, A., Yu, Y. & McCormick, D.A. Modulation of intracortical synaptic potentials by presynaptic somatic membrane potential. *Nature* **441**, 761–765 (2006).

14. Halasy, K. & Somogyi, P. Subdivisions in the multiple GABAergic innervation of granule cells in the dentate gyrus of the rat hippocampus. *Eur. J. Neurosci.* **5**, 411–429 (1993).
15. Colbert, C.M. & Johnston, D. Axonal action-potential initiation and Na^+ channel densities in the soma and axon initial segment of subicular pyramidal neurons. *J. Neurosci.* **16**, 6676–6686 (1996).
16. Palmer, L.M. & Stuart, G.J. Site of action potential initiation in layer 5 pyramidal neurons. *J. Neurosci.* **26**, 1854–1863 (2006).
17. Kim, S., Guzman, S.J., Hu, H. & Jonas, P. Active dendrites support efficient initiation of dendritic spikes in hippocampal CA3 pyramidal neurons. *Nat. Neurosci.* **15**, 600–606 (2012).
18. Baranauskas, G., David, Y. & Fleidervish, I.A. Spatial mismatch between the Na^+ flux and spike initiation in axon initial segment. *Proc. Natl. Acad. Sci. USA* **110**, 4051–4056 (2013).
19. Bean, B.P. The action potential in mammalian central neurons. *Nat. Rev. Neurosci.* **8**, 451–465 (2007).
20. Meeks, J.P. & Mennerick, S. Action potential initiation and propagation in CA3 pyramidal axons. *J. Neurophysiol.* **97**, 3460–3472 (2007).
21. Schmidt-Hieber, C., Jonas, P. & Bischofberger, J. Action potential initiation and propagation in hippocampal mossy fibre axons. *J. Physiol. (Lond.)* **586**, 1849–1857 (2008).
22. Kole, M.H.P. *et al.* Action potential generation requires a high sodium channel density in the axon initial segment. *Nat. Neurosci.* **11**, 178–186 (2008).
23. Mainen, Z.F., Joerges, J., Huguenard, J.R. & Sejnowski, T.J. A model of spike initiation in neocortical pyramidal neurons. *Neuron* **15**, 1427–1439 (1995).
24. Hodgkin, A.L. & Huxley, A.F. Currents carried by sodium and potassium ions through the membrane of the giant axon of *Loligo*. *J. Physiol. (Lond.)* **116**, 449–472 (1952).
25. Goldman, L. & Schauf, C.L. Quantitative description of sodium and potassium currents and computed action potentials in *Myxicola* giant axons. *J. Gen. Physiol.* **61**, 361–384 (1973).
26. Sigworth, F.J. The variance of sodium current fluctuations at the node of Ranvier. *J. Physiol. (Lond.)* **307**, 97–129 (1980).
27. Lorincz, A. & Nusser, Z. Cell type–dependent molecular composition of the axon initial segment. *J. Neurosci.* **28**, 14329–14340 (2008).
28. Hu, W. *et al.* Distinct contributions of $Na_v1.6$ and $Na_v1.2$ in action potential initiation and backpropagation. *Nat. Neurosci.* **12**, 996–1002 (2009).
29. Fleidervish, I.A., Lasser-Ross, N., Gutnick, M.J. & Ross, W.N. Na^+ imaging reveals little difference in action potential–evoked Na^+ influx between axon and soma. *Nat. Neurosci.* **13**, 852–860 (2010).
30. Schmidt-Hieber, C. & Bischofberger, J. Fast sodium channel gating supports localized and efficient axonal action potential initiation. *J. Neurosci.* **30**, 10233–10242 (2010).
31. Boiko, T. *et al.* Functional specialization of the axon initial segment by isoform-specific sodium channel targeting. *J. Neurosci.* **23**, 2306–2313 (2003).
32. Carter, B.C. & Bean, B.P. Sodium entry during action potentials of mammalian neurons: incomplete inactivation and reduced metabolic efficiency in fast-spiking neurons. *Neuron* **64**, 898–909 (2009).
33. Alle, H., Roth, A. & Geiger, J.R.P. Energy-efficient action potentials in hippocampal mossy fibers. *Science* **325**, 1405–1408 (2009).
34. Hodgkin, A.L. & Huxley, A.F. A quantitative description of membrane current and its application to conduction and excitation in nerve. *J. Physiol. (Lond.)* **117**, 500–544 (1952).
35. Wang, X.J. & Buzsáki, G. Gamma oscillation by synaptic inhibition in a hippocampal interneuronal network model. *J. Neurosci.* **16**, 6402–6413 (1996).
36. Rudy, B. & McBain, C.J. Kv3 channels: voltage-gated K^+ channels designed for high-frequency repetitive firing. *Trends Neurosci.* **24**, 517–526 (2001).
37. Madeja, M. Do neurons have a reserve of sodium channels for the generation of action potentials? A study on acutely isolated CA1 neurons from the guinea-pig hippocampus. *Eur. J. Neurosci.* **12**, 1–7 (2000).
38. Debanne, D., Guérineau, N.C., Gähwiler, B.H. & Thompson, S.M. Action-potential propagation gated by an axonal I_A-like K^+ conductance in hippocampus. *Nature* **389**, 286–289 (1997).
39. Soleng, A.F., Chiu, K. & Raastad, M. Unmyelinated axons in the rat hippocampus hyperpolarize and activate an H current when spike frequency exceeds 1 Hz. *J. Physiol. (Lond.)* **552**, 459–470 (2003).
40. Meeks, J.P. & Mennerick, S. Selective effects of potassium elevations on glutamate signaling and action potential conduction in hippocampus. *J. Neurosci.* **24**, 197–206 (2004).
41. Moore, J.W., Stockbridge, N. & Westerfield, M. On the site of impulse initiation in a neurone. *J. Physiol. (Lond.)* **336**, 301–311 (1983).
42. Colbert, C.M. & Pan, E. Ion channel properties underlying axonal action potential initiation in pyramidal neurons. *Nat. Neurosci.* **5**, 533–538 (2002).
43. Huxley, A.F. & Stämpfli, R. Evidence for saltatory conduction in peripheral myelinated nerve fibres. *J. Physiol. (Lond.)* **108**, 315–339 (1949).
44. Engel, D. & Jonas, P. Presynaptic action potential amplification by voltage-gated Na^+ channels in hippocampal mossy fiber boutons. *Neuron* **45**, 405–417 (2005).
45. Lapray, D. *et al.* Behavior-dependent specialization of identified hippocampal interneurons. *Nat. Neurosci.* **15**, 1265–1271 (2012).
46. Martina, M., Schultz, J.H., Ehmke, H., Monyer, H. & Jonas, P. Functional and molecular differences between voltage-gated K^+ channels of fast-spiking interneurons and pyramidal neurons of rat hippocampus. *J. Neurosci.* **18**, 8111–8125 (1998).
47. Okaty, B.W., Miller, M.N., Sugino, K., Hempel, C.M. & Nelson, S.B. Transcriptional and electrophysiological maturation of neocortical fast-spiking GABAergic interneurons. *J. Neurosci.* **29**, 7040–7052 (2009).
48. Bartos, M. *et al.* Fast synaptic inhibition promotes synchronized gamma oscillations in hippocampal interneuron networks. *Proc. Natl. Acad. Sci. USA* **99**, 13222–13227 (2002).
49. Maex, R. & De Schutter, E. Resonant synchronization in heterogeneous networks of inhibitory neurons. *J. Neurosci.* **23**, 10503–10514 (2003).
50. Traub, R.D., Whittington, M.A., Stanford, I.M. & Jefferys, J.G.R. A mechanism for generation of long-range synchronous fast oscillations in the cortex. *Nature* **383**, 621–624 (1996).

ONLINE METHODS

Axonal patch-clamp recording. Recording from axons of fast-spiking BCs of the dentate gyrus was performed according to previously established experimental protocols[12,17,51,52]. Transverse hippocampal slices (thickness of 350 µm) were prepared from the brains of 17–22-d-old Wistar rats of either sex. Rats were maintained under light (7 a.m. to 7 p.m.) and dark cycle (7 p.m. to 7 a.m.) conditions and were kept in a litter of eight rats together with the mother in a single cage. Animals were killed by rapid decapitation, in accordance with national and institutional guidelines. Experiments were approved by the Bundesministerium für Wissenschaft and Forschung (A. Haslinger, Vienna). Slices were cut in ice-cold, sucrose-containing physiological extracellular solution using a vibratome (VT1200, Leica Microsystems), incubated in a maintenance chamber filled with standard physiological extracellular solution at ~34 °C for 30 min, and subsequently stored at 22–25 °C. Slices were then individually transferred into a recording chamber superfused with standard physiological extracellular solution. Recordings were performed at 22–25 °C or, in a subset of experiments, at near-physiological temperature (30–33 °C) as indicated. In each experiment, temperature was held constant within ±0.5 °C.

For recording from interneuron axons, the following experimental strategy was implemented. First, a somatic recording was obtained, using an internal solution containing Alexa Fluor 488 (100 or 200 µM, Invitrogen). Second, after ~30 min of somatic whole-cell recording, the fluorescently labeled axon was tangentially traced from the BC soma through the granule cell layer with a Nipkow spinning disk confocal microscope (Ultraview live cell imager, PerkinElmer, equipped with an Orca camera, Hamamatsu and an argon/krypton laser, excitation wavelength of 488 nm). Exposure time was minimized to avoid phototoxic damage. Finally, fluorescent and infrared differential interference contrast (IR-DIC) images were compared and axons were patched under IR-DIC. Recordings were made from either axon shafts or small spherical axon expansions, presumably representing 'blebs' formed during the slicing procedure[13], from up to tenth order axon branches at distances of up to 418 µm from the soma. This procedure resulted in a simultaneous axon-soma recording configuration. From this configuration, axonal outside-out patches were subsequently obtained by slowly withdrawing the axonal pipette. In all cases, axons could be unequivocally distinguished from dendrites on the basis of smaller diameter, location within or adjacent to the granule cell layer, and abundance of tangential collaterals. Under our conditions, the proportion of recordings from glial cells was <10%, consistent with the absence of myelination of axons of dentate gyrus BCs[14] (**Fig. 1e** and **Supplementary Fig. 2**). For illustration and documentation purposes, 20 cells were rescanned with a Leica TCS SP5 II confocal microscope (Leica Microsystems).

Patch pipettes were fabricated from thick-walled borosilicate glass tubing (outer diameter = 2 mm, inner diameter = 1 mm) with a horizontal pipette puller (P-97, Sutter Instruments). When filled with internal solution, they had a resistance of 2–10 MΩ for somatic recording and 10–32 MΩ for axonal recording. For outside-out patch experiments to measure Na^+ channel density, pipettes with a resistance of 4.9–32 MΩ were used. Current- and voltage-clamp recordings were performed using a Multiclamp 700B amplifier (Molecular Devices). In BC recordings, series resistance was 15–90 MΩ. Cells with somatic resting potentials more positive than −50 mV were discarded. Pipette capacitance and series resistance compensation (bridge balance) were applied throughout current-clamp experiments. Bridge balance was monitored and readjusted as required. BCs were held at a membrane potential of ~−65 mV, injecting a holding current at the soma (range = −150 to +200 pA) or at the axon (range = −20 to −100 pA).

Signals were low-pass filtered at 10 kHz (voltage traces) and 4 or 10 kHz (current traces), and sampled at 20–100 kHz with a CED power interface (Cambridge Electronic Design). Pulse protocols were generated using custom-made data acquisition software (FPulse versions 3.19 and 3.33, U. Fröbe, University of Freiburg) running under Igor 6.20 (WaveMetrics). In a subset of experiments, Na^+ currents were pharmacologically isolated with 5–20 mM tetraethylammoniumchloride (TEA), 1–10 mM 4-aminopyrididine (4-AP), and 0.1 mM $CdCl_2$ added to the bath solution. To measure the peak amplitude of voltage-gated Na^+ current in outside-out patches, a pulse sequence composed of a 50-ms prepulse to −120 mV followed by a 30- or 100-ms test pulse to 0 mV was generated. For activation and inactivation protocols, prepulse and test pulse durations were the same, whereas amplitudes were varied as indicated. The holding potential before and after the pulse sequence was −90 mV. Voltage protocols were applied to outside-out patches once every 3–15 s. Leak and capacitive currents were subtracted online using a 'P over −4' or 'P over −8' correction procedure.

BCs were identified based on the non-accommodating, fast-spiking AP phenotype (average AP frequency >50 Hz at 22–25 °C and >150 Hz at near-physiological temperature in response to 1-s, 0.3–1-nA somatic current pulses), and the localization of the axonal arbor, which was largely restricted to the granule cell layer in the confocal image. Identification during the experiment was confirmed by *post hoc* biocytin labeling (**Fig. 1b**). Detailed light-microscopic analysis of the axonal arbor revealed that the majority of cells were classical BCs with tangential collaterals, forming basket-like structures around granule cell somata[12].

Paired BC–granule cell (GC) recordings. To examine the effects of Na^+ channel block on synaptic latency, paired recordings were made between synaptically connected BCs and GCs[53] (**Supplementary Fig. 9**). In this set of experiments, the distance between somata of pre- and postsynaptic neurons was 219 ± 14 µm, and the recording temperature was 22–25 °C. Series resistance in the postsynaptic GC was 6–14 MΩ and remained stable in each experiment. GCs were voltage-clamped at −80 mV without series resistance compensation. Latency was measured from the time point of the half-maximal amplitude of the presynaptic AP to the onset of the IPSC.

Solutions and chemicals. The standard physiological extracellular solution contained 125 mM NaCl, 25 mM $NaHCO_3$, 2.5 mM KCl, 1.25 mM NaH_2PO_4, 2 mM $CaCl_2$, 1 mM $MgCl_2$ and 25 mM D-glucose (equilibrated with 95% O_2 and 5% CO_2 gas mixture). For BC axon-soma whole-cell and outside-out patch recordings, the intracellular solution contained 120 mM potassium gluconate, 20 mM KCl, 10 mM EGTA, 2 mM $MgCl_2$, 2 mM Na_2ATP, 10 mM HEPES and 0.2% biocytin, pH adjusted to 7.3 with KOH. In a subset of experiments, 0.1 mM spermine was added to the internal solution. 100–200 µM Alexa Fluor 488 (Invitrogen) was added to the internal solution for all somatic recording electrodes. For BC-GC paired recordings, the internal solution for the presynaptic BC contained 135 mM potassium gluconate, 20 mM KCl, 0.1 mM EGTA, 2 mM $MgCl_2$, 2 mM Na_2ATP, 10 mM HEPES and 0.2% biocytin, whereas the solution for the postsynaptic GC contained 145 mM KCl, 0.1 mM EGTA, 2 mM $MgCl_2$, 2 mM Na_2ATP and 10 mM HEPES, pH adjusted to ~7.3 with KOH. TEA, 4-AP, and $CdCl_2$ were from Sigma-Aldrich, TTX was from Alomone Labs.

Immunohistochemistry. Immunolabeling of neurons in the dentate gyrus was performed according to previously established protocols[54]. Rats (17–22 d old, covering the range used in electrophysiology experiments; **Fig. 1e**; or ~6 weeks old; **Supplementary Fig. 2**) were intracardially perfused with phosphate-buffered saline (PBS, composed of 137 mM NaCl, 2.7 mM KCl, 10 mM Na_2HPO_4, and 1.8 mM KH_2PO_4, pH 7.4) for 5 min and subsequently with 1% paraformaldehyde (PFA, wt/vol) and 1% sucrose (wt/vol) in PBS. After a postfixation of 2 h in 1% PFA and 1% sucrose in PBS and a subsequent incubation in 30% sucrose in phosphate-buffered solution (PB, 0.1 M, pH 7.35) for 12 h, 50-µm-thick slices were cut with a vibratome at −18 °C. Slices were washed (3 × 10 min) with PBS and subsequently incubated in 10% normal goat serum (vol/vol) for 1 h. They were then incubated for 24 h at 22–25 °C with a rabbit polyclonal antibody to parvalbumin (PV-25, 1:1,000, Swant) and a mouse monoclonal antibody to myelin basic protein (MBP, SMI99P-100, 1:1,000, Sternberger Monoclonals) in PBS containing 5% normal goat serum and 0.3% Triton X-100 (wt/vol). The antibody to parvalbumin was previously confirmed in PV knockout mice[54] and the antibody to MBP had been previously validated in Long Evans Shaker rats[55]. After washing, slices were incubated for 12 h at 4 °C with goat antibody to rabbit Alexa Fluor 488 and goat antibody to mouse Alexa Fluor 647 (both 1:1,000, Invitrogen) in PBS containing 3% normal goat serum and 0.3% Triton X-100. Finally, slices were embedded in Prolong Gold Antifade (Invitrogen) and examined using a Leica TCS SP5 II confocal microscope (Leica Microsystems). Experiments were repeated on five animals for each age group, giving consistent results. Although the dentate gyrus granule cell layer was devoid of MBP immunoreactivity, strong immunolabeling was detected in stratum oriens-alveus and fimbria in adjacent CA3 and CA1 subfields. Furthermore, although PV and MBP colocalization was completely absent in the dentate gyrus granule cell layer, slight colocalization was detected in CA3 and CA1 pyramidal cell layer[56].

Data analysis. Analysis was performed using Stimfit 0.9.2–0.13.2 (C. Schmidt-Hieber, University College London, and José Guzmán, Institute of Science and Technology Austria), Clampfit 9 (Molecular Devices), Origin (Microcal) and Excel (Microsoft). AP amplitude was measured from threshold (40 V s^{-1}). Latency differences between somatic and axonal APs were quantified using the time points corresponding to half-maximal amplitude in the AP rising phase. To determine the AP initiation site, latency–distance data were fit with a bilinear function with sigmoidal transition of the form $L(x) = (1 - f(x))ax + f(x)(bx + c)$, where L is latency, x is distance, a and b are slope factors, c is an offset, and $f(x)$ is a sigmoidal (Boltzmann-like) function. AP propagation velocity was obtained as $1/b$. For the experiments at near-physiological temperature, c was set to 0 to reduce the number of free parameters. Experiments in which the axon originated from one of the dendrites were excluded from this analysis (30 recordings in **Fig. 2c** and four recordings in **Supplementary Fig. 3c**).

Na^+ channel activation curves were determined by calculating chord conductance values (g) from peak currents, assuming ohmic behavior and a reversal potential of 70 mV[57]. Na^+ conductance density ($\overline{g_{Na}}$) was calculated based on the peak current at 0 mV and the open probability at this membrane potential determined by nonstationary fluctuation analysis. Activation and inactivation curves were fit by a Boltzmann function

$$f = 1/(1 + \exp((V_{1/2} - V)/k))$$

where V is the membrane potential, $V_{1/2}$ is the midpoint potential and k is the slope factor. Na^+ current activation time constant was obtained by fitting rise and early decay of the Na^+ current with a function of the form $I(t) = (1 - \exp(-(t - \delta)/\tau_m))(a\exp(-(t - \delta)/\tau_h) + b)$ for $t > \delta$ and $I(t) = 0$ for $t \leq \delta$, where δ is a delay, τ_m is activation time constant, τ_h is inactivation time constant, and a and b are amplitude values. Na^+ current inactivation time constant was obtained by fitting the decay phase of the Na^+ current with a single exponential. Na^+ current deactivation time constant was either fit with a single exponential (at test voltage < −50 mV) or a biexponential function (at test voltage ≥ −50 mV); in the latter case, the deactivation time constant was taken from the fast component[58]. Na^+ channel single-channel conductance and open probability at the peak were estimated by nonstationary fluctuation analysis[26,44]. To minimize the effects of rundown, data were analyzed in blocks of ten traces each. Variance-mean data were fit with a parabolic function

$$\sigma^2(I) = iI - I^2/N + \sigma_0^2$$

where σ^2 is mean variance, I is the mean current, i is the single-channel current, N is the number of available channels in the patch, and σ_0^2 is the baseline variance[26,44].

Membrane potentials are specified without correction for liquid junction potentials. Values indicate mean ± s.e.m. Error bars in figures also indicate s.e.m. No statistical methods were used to pre-determine sample sizes. Traces of Na^+ currents shown in figures represent averages of 5–100 individual traces (except **Fig. 3d**). To account for the effects of low-pass filtering, traces were shifted by 32.9 µs with respect to the voltage pulse protocol[44]. Significance of differences of mean values was assessed by a two-sided nonparametric Wilcoxon signed rank test or Wilcoxon rank sum test. Significance of differences of activation and inactivation curves was assessed with a bootstrap method[44]. The significance level of statistic tests was set to $P < 0.05$. Distances were measured from the point of origin of the axon to the axonal recording site along the axonal trajectory in the fluorescent image, after sections at different focal planes had been merged following each experiment. To assess the possibility of a systematic bias between axon shaft and axon bleb recordings, we compared residuals $y_i - f(x_i)$ between the two data sets (where x_i, y_i are the coordinates of each data point and $f(x)$ represents the function fit to the total data set); no statistical differences were observed (latency-distance data, $P > 0.2$; **Fig. 2c**; $\overline{g_{Na}}$ distance data, $P > 0.05$; **Fig. 3b**).

For estimation of current and channel density, membrane patch area was estimated from the pipette resistance using a linear relation between patch area and pipette conductance (**Supplementary Fig. 4**). In a subset of outside-out patches (seven axon and nine soma recordings), capacitance was directly measured by recording capacitive transients from outside-out patches before and after pushing the pipette tip gently into an insulating ball of silicone elastomer[44,59] (Sylgard 184, Dow Corning). A contribution from the pipette was corrected, assuming a pipette capacitance of 1 pF mm^{-1} and an insertion depth of 10 µm.

To compare different Na^+ conductance distributions (for example, the nested models $f(x)$ and $g(x)$), the sum of squared errors (SSE) between experimental data and model was calculated, and $[(SSE_f - SSE_g)/k_f] / [SSE_g/(n - k_g)]$ was compared with $F(k_f, n - k_g)$, where F is the F distribution, n is the number of data points, and k_f and k_g are the degrees of freedom[60]. Nonnested models were compared with a bootstrap method[60].

Computational model of AP initiation and propagation in BC axons. Simulation of AP initiation and propagation was performed using NEURON 7.1 (ref. 61) in combination with Mathematica 8.01 (Wolfram Research) running under Windows XP x64 on a Lian Li desktop computer (72 GByte RAM) or under Windows 7 on a PC. Simulations were performed on detailed passive cable models of BCs taken from a previously published sample[9] (cell 2, 1,017 sections total, or other cells from the sample as indicated). Neurons had been filled with biocytin during recording, stained with 3,3′-diaminobenzidine, and fully reconstructed (including soma, dendrites, and entire axon) using a Neurolucida reconstruction system, as described previously[9]. In the morphometrically detailed model, the specific cable parameters were set according to approximate average values (R_m = 10 kΩ cm^2, C_m = 0.9 µF cm^{-2} and R_i = 170 Ω cm). Nonlinear capacitive currents were not included, as their effect on AP propagation is expected to be minimal for physiologically relevant channel density values[62]. To simplify the stability properties of the model, a high value of I_h conductance in the BC axon[63] was lumped into a uniform axonal R_m value of 10 kΩ cm^2. The integration time step was set to 5 µs. Na^+ and K^+ channels were inserted using the previously published Wang and Buzsáki (WB) model[35]. WB channels were chosen, as they robustly confer a fast-spiking AP phenotype in single-compartment models[35]. $\overline{g_{Na}}$ was set to 100 pS $µm^{-2}$ at the dendrite, 200 pS $µm^{-2}$ at the soma, and between 200 and 2,000 pS $µm^{-2}$ in the axon. The maximal K^+ conductance $\overline{g}_K$ was uniformly set to 300 pS $µm^{-2}$ in dendrites, soma, and axon. The reversal potential of the leak conductance was chosen as −70 mV. The border between proximal and distal axonal compartments was set at 120-µm distance from the center of the soma. Reliability of AP propagation was quantified as the ratio of the number of spikes in the first axonal segment (immediately adjacent to the soma) and that at a given axonal location. Spikelets with absolute peak amplitude < −40 mV were discarded from the count. Latency differences between somatic and axonal APs were quantified using the time points corresponding to the maximal rate of rise of the AP. Path distance was measured from the center of the soma. In all simulations, APs were evoked by brief or long current pulses (1–4 nA, 1 ms or 500 ms). For simulations with a schematic ball-and-stick model (**Supplementary Fig. 1**), both specific cable parameters (R_m = 10 kΩ cm^2, C_m = 0.9 µF cm^{-2}, and R_i = 170 Ω cm) and active conductances (WB) were chosen to be the same as those in the detailed models.

51. Bischofberger, J., Engel, D., Li, L., Geiger, J.R.P. & Jonas, P. Patch-clamp recording from mossy fiber terminals in hippocampal slices. *Nat. Protoc.* **1**, 2075–2081 (2006).
52. Nevian, T., Larkum, M.E., Polsky, A. & Schiller, J. Properties of basal dendrites of layer 5 pyramidal neurons: a direct patch-clamp recording study. *Nat. Neurosci.* **10**, 206–214 (2007).
53. Kraushaar, U. & Jonas, P. Efficacy and stability of quantal GABA release at a hippocampal interneuron-principal neuron synapse. *J. Neurosci.* **20**, 5594–5607 (2000).
54. Eggermann, E. & Jonas, P. How the 'slow' Ca^{2+} buffer parvalbumin affects transmitter release in nanodomain coupling regimes at GABAergic synapses. *Nat. Neurosci.* **15**, 20–22 (2012).
55. Kim, J.H., Renden, R. & von Gersdorff, H. Dysmyelination of auditory afferent axons increases the jitter of action potential timing during high-frequency firing. *J. Neurosci.* **33**, 9402–9407 (2013).
56. McGee, A.W., Yang, Y., Fischer, Q.S., Daw, N.W. & Strittmatter, S.M. Experience-driven plasticity of visual cortex limited by myelin and Nogo receptor. *Science* **309**, 2222–2226 (2005).
57. Martina, M. & Jonas, P. Functional differences in Na^+ channel gating between fast-spiking interneurones and principal neurones of rat hippocampus. *J. Physiol. (Lond.)* **505**, 593–603 (1997).
58. Oxford, G.S. Some kinetic and steady-state properties of sodium channels after removal of inactivation. *J. Gen. Physiol.* **77**, 1–22 (1981).
59. Sakmann, B. & Neher, E. Geometric parameters of pipettes and membrane patches. in *Single-Channel Recording, 2nd edn* (eds. Sakmann, B. & Neher, E.) 637–650 (Plenum Press, New York/London, 1995).
60. Horn, R. Statistical methods for model discrimination. Applications to gating kinetics and permeation of the acetylcholine receptor channel. *Biophys. J.* **51**, 255–263 (1987).
61. Carnevale, N.T. & Hines, M.L. *The Neuron Book* (Cambridge University Press, Cambridge, 2006).
62. Hodgkin, A. The optimum density of sodium channels in an unmyelinated nerve. *Phil. Trans. R. Soc. Lond. B* **270**, 297–300 (1975).
63. Aponte, Y., Lien, C.C., Reisinger, E. & Jonas, P. Hyperpolarization-activated cation channels in fast-spiking interneurons of rat hippocampus. *J. Physiol. (Lond.)* **574**, 229–243 (2006).

doi:10.1038/nn.3678

A supercritical density of Na^+ channels ensures fast signaling in GABAergic interneuron axons

Hua Hu & Peter Jonas

IST Austria, Klosterneuburg, Austria

Corresponding authors:
Dr. Peter Jonas
Dr. Hua Hu
IST Austria
Am Campus 1
A-3400 Klosterneuburg
Austria
Phone: ++43-2243-9000-3701
Fax: ++43-2243-9000-2007
E-mail: peter.jonas@ist.ac.at, hua.hu@ist.ac.at

Nature Neuroscience: doi:10.1038/nn.3678

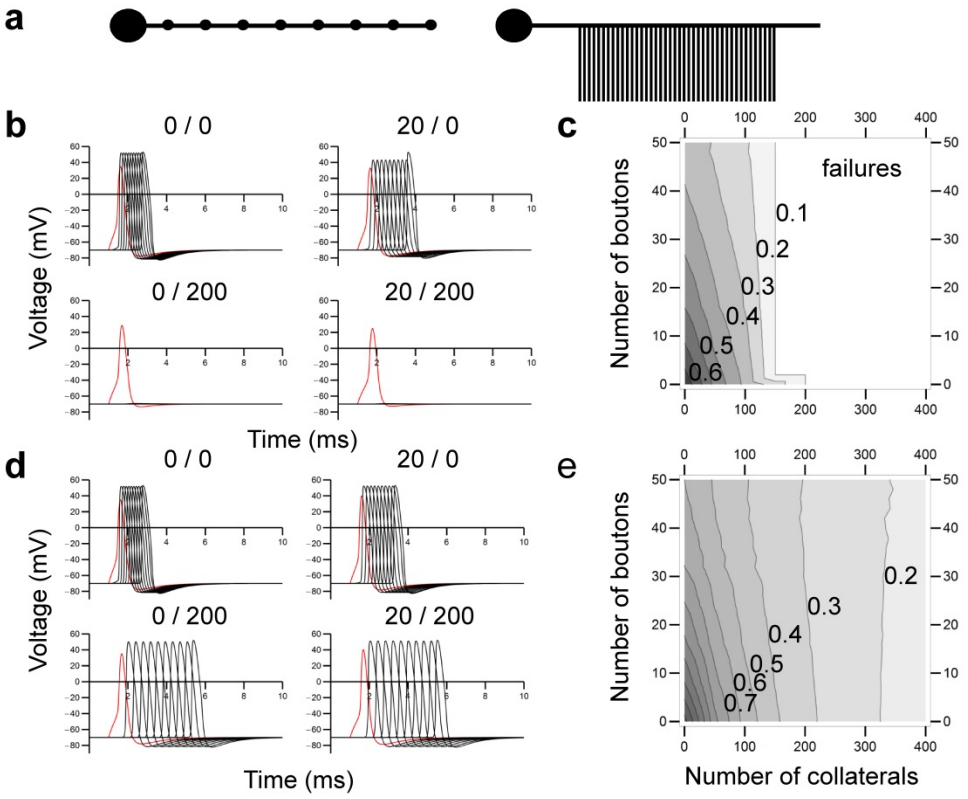

Supplementary Figure 1 High density of boutons and axon collaterals generates failures and slowing of propagation of APs in schematic models.

(**a**) Structure of the schematic model. Large sphere on the left represents soma (20 µm diameter), horizontal cylinder on the right is axon (1 mm length; 0.5 µm diameter), small spheres represent boutons (5 µm diameter), and vertical cylinders indicate axon collaterals (100 µm length; 0.3 µm diameter). Throughout the simulations, $\overline{g_{Na}}$ in the soma was 200 pS µm^{-2}, and $\overline{g_{Na}}$ in the axon was 1200 pS µm^{-2}. Boutons and collaterals were introduced with equidistant spacing. Axon diameters were approximately consistent with previous electron microscopy data[14].

(**b**) APs evoked by a short current pulse at the soma (1 nA, 1 ms). Red trace, somatic AP, black traces, APs in the axon at different sites with 100 µm distance. Numbers on top indicate the number of boutons / number of collaterals.

(**c**) Contour plot of AP propagation velocity against number of boutons and number of axon collaterals. Note failure of AP propagation in a large part of the parameter space. In both **b** and **c**, passive properties of boutons and collaterals were assumed ($\overline{g_{Na}}$ = 0).

(**d, e**) AP traces (**d**) and contour plot of AP propagation velocity (**e**) in the case of active boutons and collaterals ($\overline{g_{Na}}$ = 1200 pS µm^{-2}).

Numbers right-adjacent to contour lines in **c** and **e** indicate AP propagation velocity (in m s^{-1}).

Nature Neuroscience: doi:10.1038/nn.3678

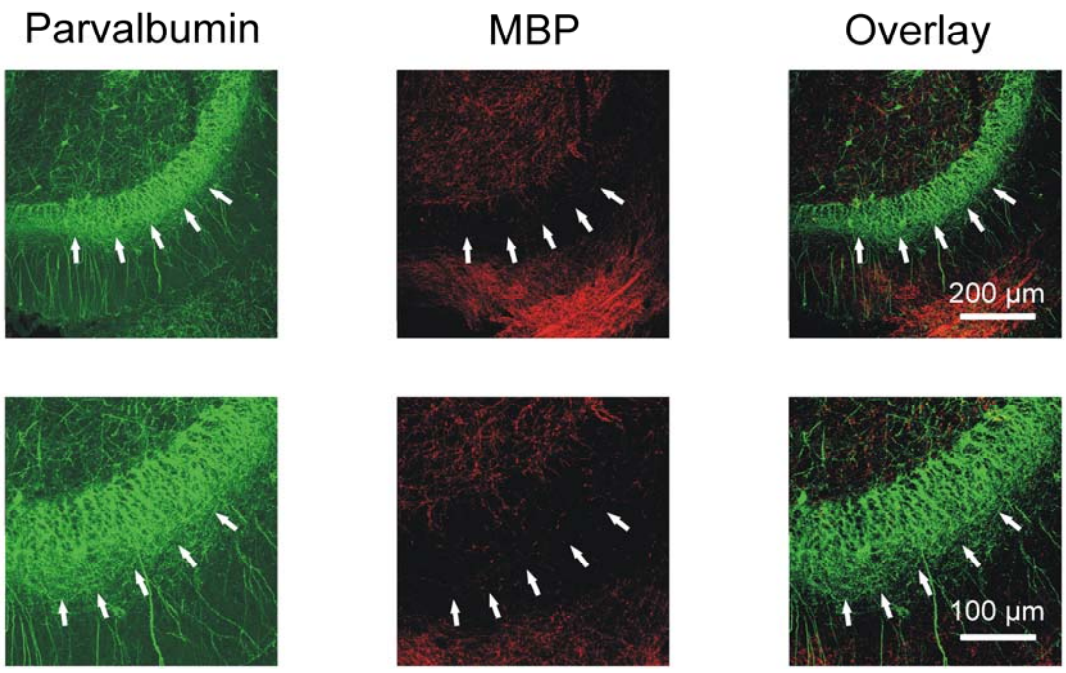

Supplementary Figure 2 Minimal myelination of BC axons in dentate gyrus of ~6-weeks-old rats.
Double immunolabeling for parvalbumin and myelin basic protein (MBP) in a 6-week-old rat. Left, parvalbumin; center, MBP; right, overlay. Note the absence of colocalization between the two markers in the granule cell layer, suggesting that BC axons are largely unmyelinated. Experiments were repeated on 5 animals, giving consistent results. White arrows indicate the outer border of the granule cell layer. Lower micrographs are expanded versions of upper images.

Nature Neuroscience: doi:10.1038/nn.3678

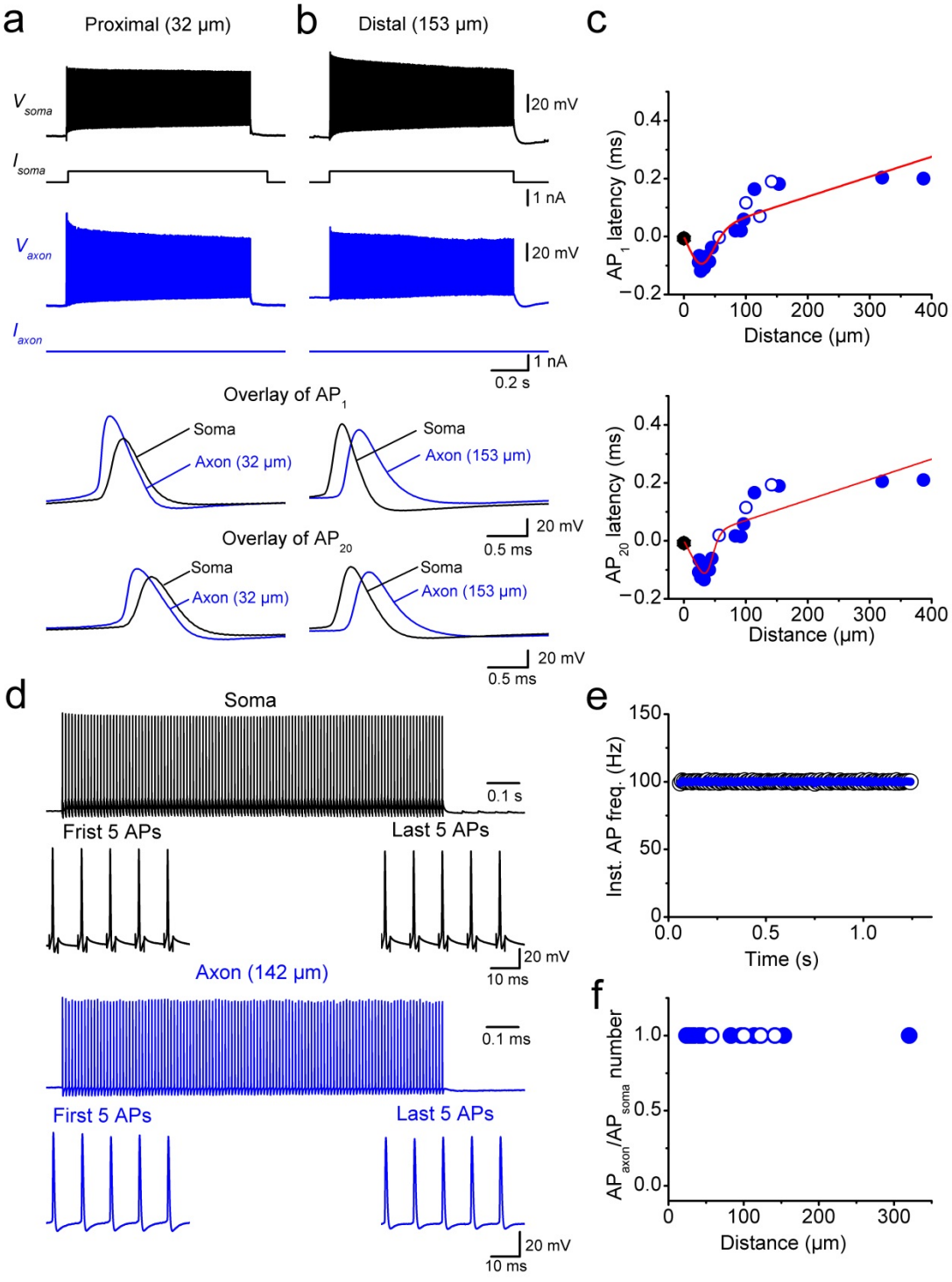

Nature Neuroscience: doi:10.1038/nn.3678

Supplementary Figure 3 Proximal initiation and fast, reliable propagation of APs in interneuron axons at near-physiological temperature.

(**a, b**) Simultaneous recording from the soma and the axon of a fast-spiking, parvalbumin-expressing BC during a long somatic current pulse. Black, somatic voltage; blue, axonal voltage. The axonal recording site was located 32 µm (**a**) or 153 µm (**b**) from the soma. Bottom traces show expanded views of the first and the 20th AP in the high-frequency train. Black traces, somatic voltage and corresponding current; blue traces, axonal voltage and corresponding current.

(**c**) Plot of latency between somatic and axonal AP against distance of the axonal recording site from the soma for the first AP (upper graph) and the 20th AP (lower graph). Data from 19 simultaneous axon–soma recordings. Filled circles, recordings from axon varicosities; open circles, recordings from axon shafts; red line, bilinear function fit to the data points.

(**d**) Simultaneous recording from the soma and the axon of a BC during a high-frequency train of short somatic current pulses (100 Hz, 120 stimuli; 3 ms, 1 nA). Black, somatic voltage; blue, axonal voltage. The axonal recording site was located 142 µm from the soma.

(**e**) Plot of instantaneous somatic and axonal AP frequency during the stimulation train. The axonal AP frequency was 100 Hz, identical to the stimulation frequency.

(**f**) Plot of ratio of number of APs in the axon over number of APs in the soma, plotted against distance of the axonal recording site. Data from 18 simultaneous axon–soma recordings. Note that the ratio was 1 in all cases, indicating high reliability of propagation.

Nature Neuroscience: doi:10.1038/nn.3678

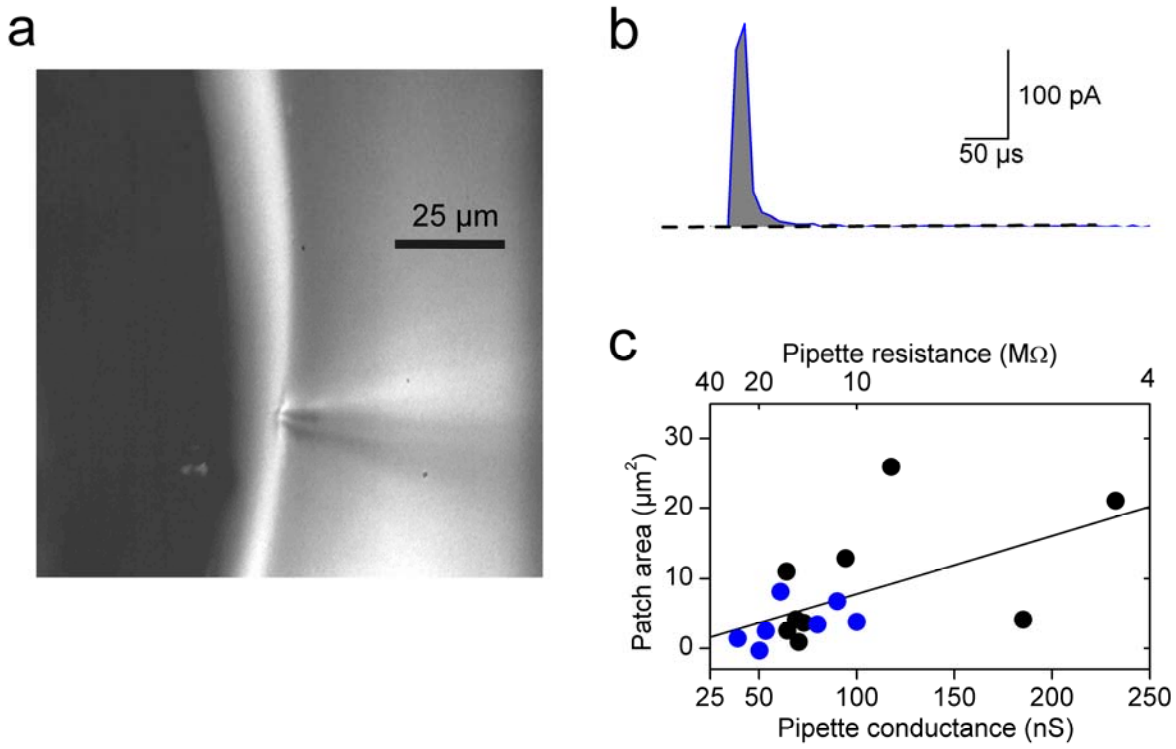

Supplementary Figure 4 Patch area determined by capacitance measurements.
(**a**) Experimental configuration. The silicone elastomer ball is visible on the left, the patch pipette is located on the right. The pipette tip was gently pushed into the insulating ball, with an insertion depth of ~10 µm.
(**b**) Difference current before and after pressing the pipette tip with the outside-out patch into the Sylgard ball. Shaded area indicates integral under the current trace. Currents were evoked by a test pulse to –100 mV from a holding potential of –50 mV.
(**c**) Plot of patch area against pipette conductance. Data were fit by linear regression, with the parameters $A(g_P) = 0.08271 \times g_P - 0.47526$, where A is patch area (μm^2) and g_P is pipette conductance (nS). Patch area was calculated from capacitance, assuming a specific membrane capacitance of 1 µF cm^{-2}. The upper horizontal axis shows pipette resistance (which is the inverse of pipette conductance). Results were obtained from 7 axonal and 9 somatic outside-out patches. Somatic data are shown in black, axonal data are depicted in blue.

Nature Neuroscience: doi:10.1038/nn.3678

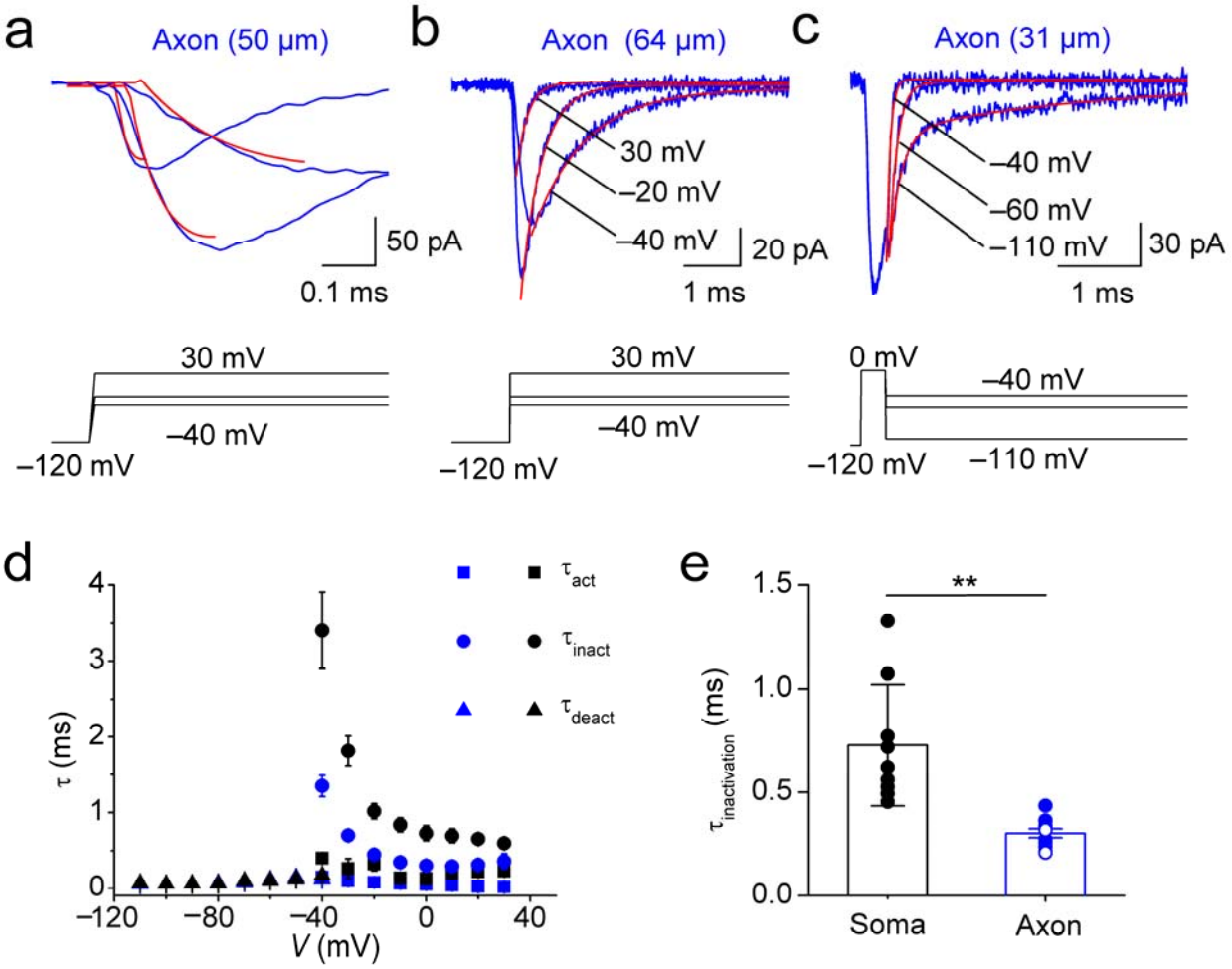

Supplementary Figure 5 Fast gating of Na^+ channels in BC axons.
(**a**–**c**) Activation (**a**), inactivation (**b**), and deactivation time course of axonal Na^+ channels (**c**). Outside-out patches isolated from the axon 50, 64, and 31 µm from the soma. Red curves indicate exponential functions fit to the recorded traces. The corresponding pulse protocol is shown at the bottom.
(**d**) Plot of activation (squares), inactivation (circles), and deactivation time constants (triangles) against test pulse potential.
(**e**) Summary bar graph of inactivation time constant at 0 mV. Bars indicate mean ± SEM, circles represent data from individual experiments (9 somatic and 11 axonal patches). Note the marked difference in the inactivation time constants between somatic and axonal Na^+ channels. ** indicates $P < 0.01$. Somatic data are shown in black, axonal data are depicted in blue.

Nature Neuroscience: doi:10.1038/nn.3678

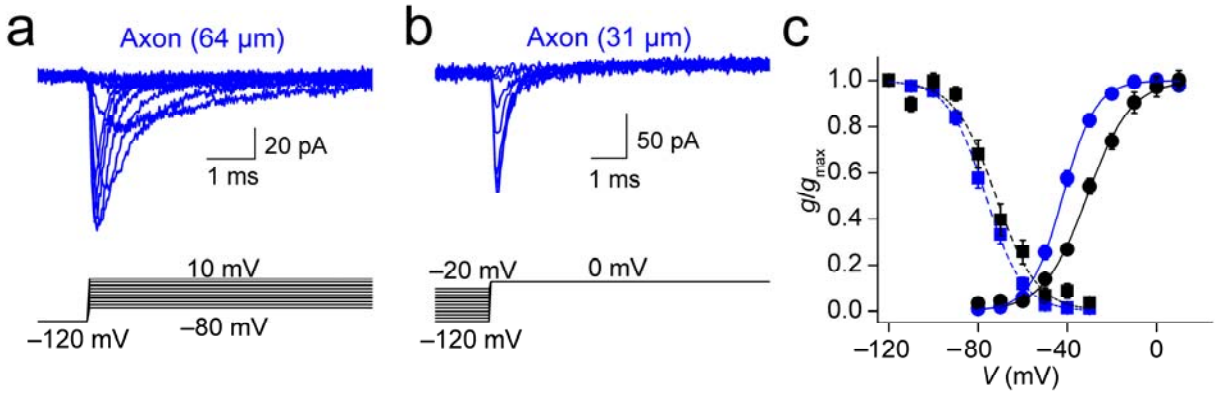

Supplementary Figure 6 Negative shift of voltage-dependence of Na^+ channel activation and inactivation in BC axons.

(**a**) Na^+ currents in an outside-out patch isolated from the axon 64 µm from the soma. The corresponding activation pulse protocol with increasing test pulse amplitude is shown at the bottom.

(**b**) Na^+ currents in an outside-out patch isolated from the axon 31 µm from the soma. The corresponding inactivation pulse protocol with increasing prepulse amplitude is shown at the bottom.

(**c**) Na^+ channel activation and inactivation curves. Data points indicate mean ± SEM from 6–14 patches. Data points were fit with Boltzmann functions. Note that the activation curve of axonal Na^+ channels is shifted to the left in comparison to that of somatic Na^+ channels. Somatic data are shown in black, axonal data are depicted in blue. Continuous and dashed lines represent Boltzmann functions fit to activation and inactivation data points, respectively.

Nature Neuroscience: doi:10.1038/nn.3678

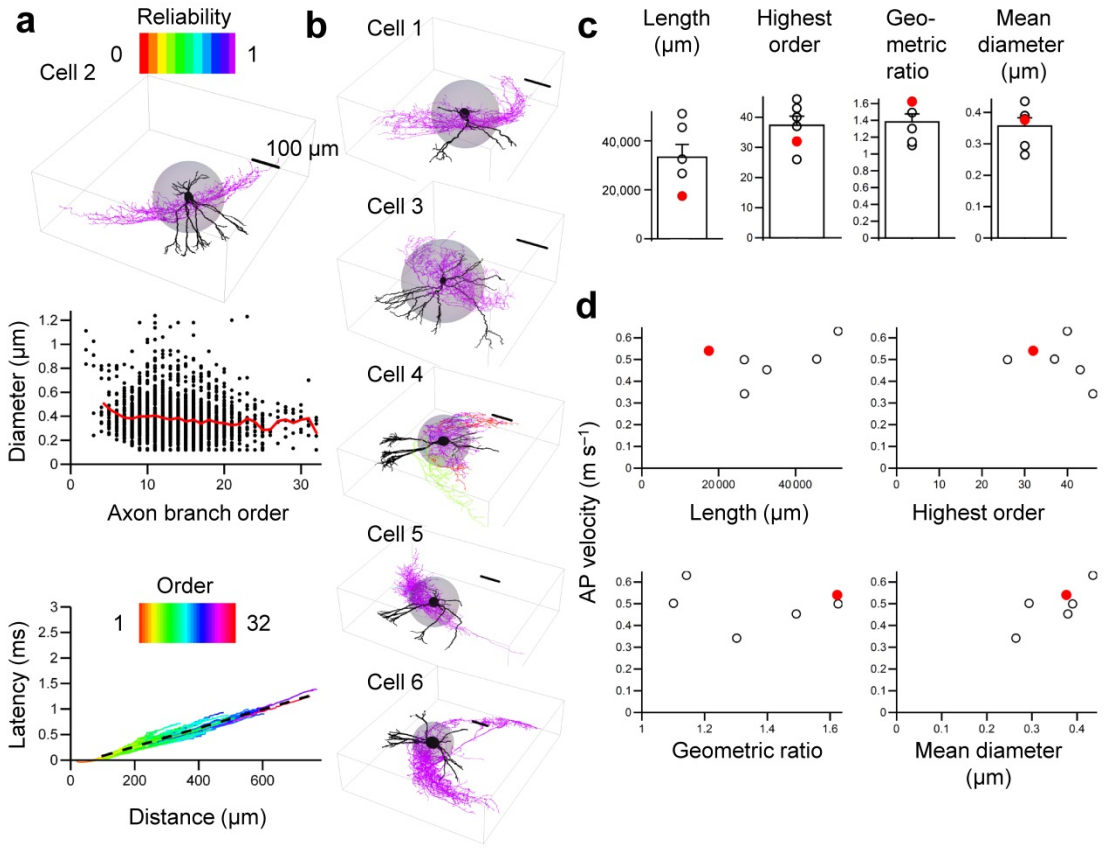

Supplementary Figure 7 Dependence of reliability and velocity of AP propagation on axonal Na^+ conductance density is independent of details of morphological properties.

(**a**) AP propagation in cell 2, used for the computational analysis in Fig. 4. Top, plot of reliability of AP propagation, shown as color coding of the surface of the reconstructed neuron for proximal $\overline{g_{Na}}$ = distal $\overline{g_{Na}}$ = 500 pS µm^{-2}. Color scale bar indicates the reliability of propagation in the axon (inset, top).

Center, plot of axon diameter against axon branch order. Black points indicate diameters of individual sections, red line represents mean.

Bottom, plot of latency against distance. Note that the slope of the latency–distance relation is constant over a wide range of distances and branch orders, indicating constant AP propagation velocity. Proximal $\overline{g_{Na}}$ = distal $\overline{g_{Na}}$ = 1000 pS µm^{-2}. Dashed line indicates the results of linear regression for distances > 100 µm. Color scale bar indicates axon branch order (inset, top).

(**b**) AP propagation in 5 other fully reconstructed BCs. Note that all cells except one (cell 4, center) showed absolute reliability of propagation; proximal $\overline{g_{Na}}$ = distal $\overline{g_{Na}}$ = 500 pS µm^{-2}.

(**c**) Structural properties of BC axons in the fully reconstructed cells. Bars indicate mean ± SEM, circles represent data from individual experiments.

(**d**) Plot of AP propagation velocity against structural parameters of BC axons. Red points in **c** and **d** indicate cell 2 used for the simulations in Fig. 4. This cell was chosen because its axon diameter was most representative.

Nature Neuroscience: doi:10.1038/nn.3678

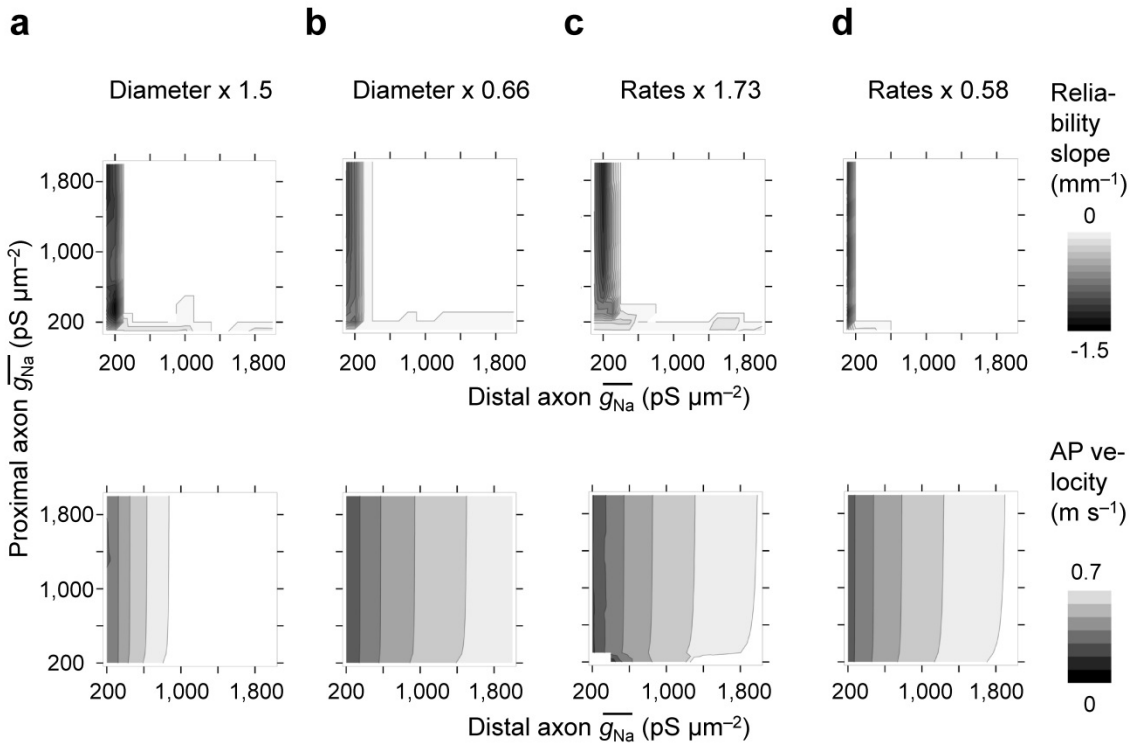

Supplementary Figure 8 Dependence of reliability and velocity of AP propagation on axon diameter and channel gating kinetics.
(**a**) Effects of increase in axon diameter (multiplying all diameters by a factor of 1.5).
(**b**) Effects of decrease in axon diameter (multiplying all diameters by a factor of 0.66).
(**c**) Effects of accelerating Na^+ channel inactivation rates and K^+ channel activation rates (multiplying corresponding rates by a factor of 1.73, corresponding to a 5°C temperature increase for a Q_{10} of 3).
(**d**) Effects of slowing Na^+ channel inactivation rates and K^+ channel activation rates (multiplying corresponding rates by a factor of 0.58, corresponding to a 5°C temperature decrease for a Q_{10} of 3).
Upper graphs, contour plots of the average slope of the reliability–distance relation as a function of proximal and distal $\overline{g_{Na}}$.
Lower graphs, contour plots of AP propagation velocity as a function of proximal and distal $\overline{g_{Na}}$.
Gray scale bar indicates the value of the indicated parameter (right). All simulations were performed on cell 2. Parameters of the simulations were identical to those in Fig. 4, unless specified differently.

Nature Neuroscience: doi:10.1038/nn.3678

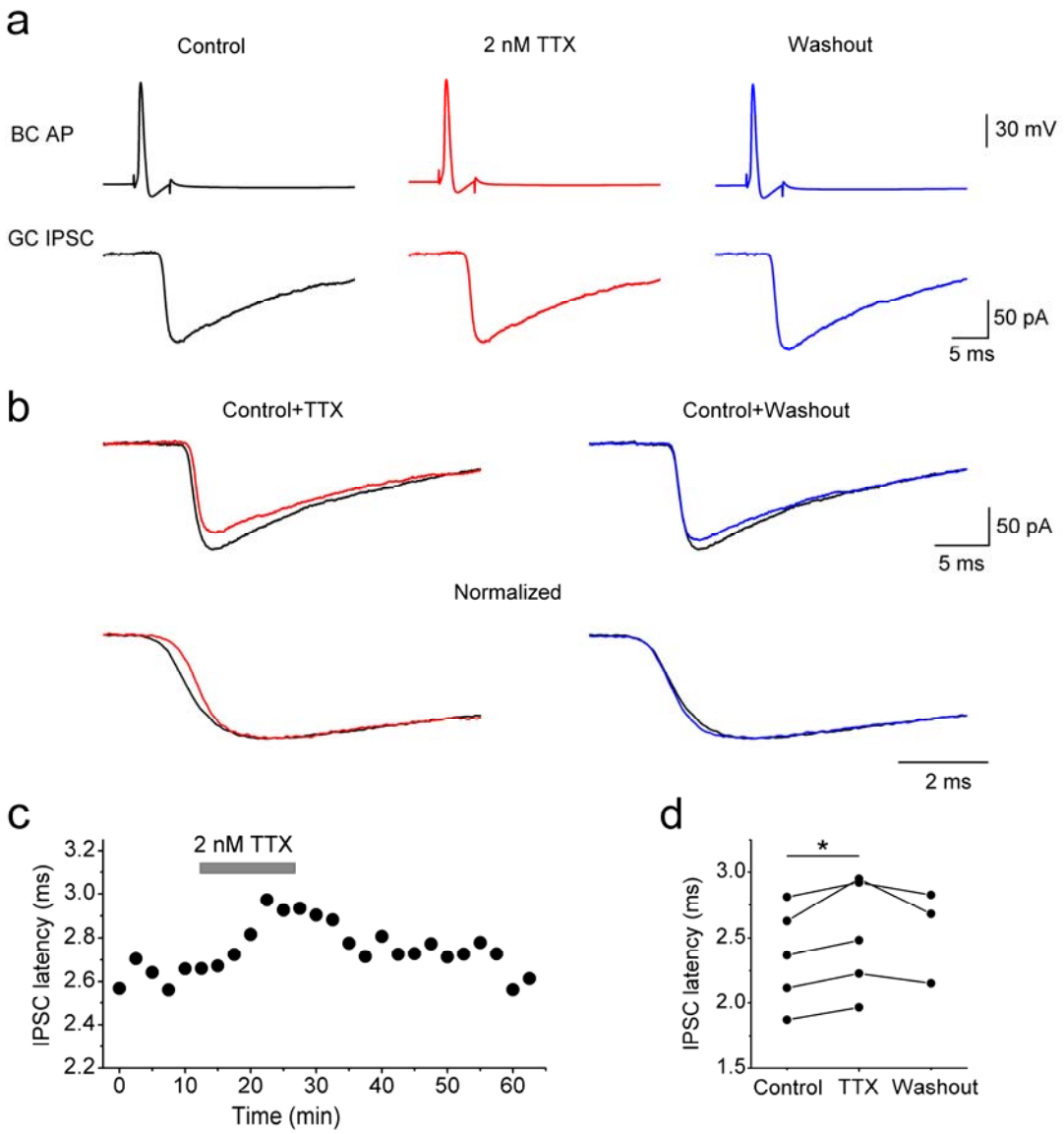

Supplementary Figure 9 Partial block of Na^+ channels increases latency of evoked IPSCs at BC–GC synapses.

(**a**) Unitary IPSCs at BC–GC synapses under control conditions (left), in the presence of 2 nM TTX in the bath (center), and after washout (right). Upper traces, APs in BCs evoked by brief current pulses; bottom traces, average IPSCs.

(**b**) Overlay of traces in control and 2 nM TTX (left) and control and washout (right) at different time scales. Note that 2 nM TTX reversibly increased the latency of evoked IPSCs. Upper traces are displayed at absolute current scale, lower traces are shown normalized to the same peak amplitude to facilitate comparison of synaptic latency.

(**c**) Plot of IPSC latency against experimental time during application of 2 nM TTX (horizontal bar) from the same experiment as shown in (**a, b**). Each data point represents the mean of 25 consecutive IPSC latency values.

(**d**) Summary graph of the effects of 2 nM TTX on IPSC latency. Data from 5 BC–GC pairs. Data from the same experiment were connected by lines. * indicates $P < 0.05$. Slight differences in the 20–80% rise time (**b**) were not significant ($P > 0.1$).

Nature Neuroscience: doi:10.1038/nn.3678

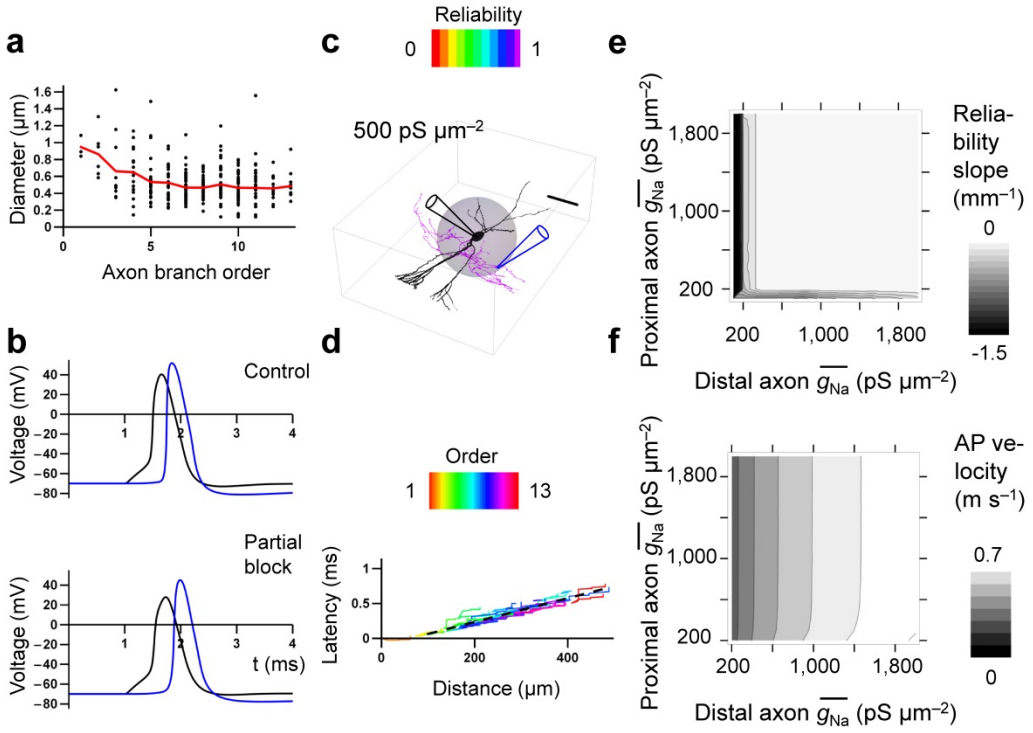

Supplementary Figure 10 A supercritical Na^+ channel density in the axon ensures fast AP propagation in an experimentally recorded cell.
(**a**) Plot of axon diameter against axon branch order in the experimentally recorded cell. Same cell as shown in **Fig. 5d**, open circles. Black points indicate diameter of individual sections, red line represents mean. Note that the axon could be only partially reconstructed.
(**b**) Simulated APs at the soma (black) and the axonal recording site (blue) under control conditions (top) and after simulated block of 43.1% of conductance (bottom). $\overline{g_{Na}}$ = 600 pS µm^{-2} and 341 pS µm^{-2}, respectively. Note that the latency between the two voltage signals increases, as observed experimentally.
(**c**) Plot of reliability of AP propagation, shown as color coding of the surface of the reconstructed neuron for $\overline{g_{Na}}$ = 500 pS µm^{-2}. Color scale bar indicates the reliability of propagation in the axon (inset, top); dendrites are depicted in black to indicate lack of active AP propagation. Gray sphere represents the proximal region of the axon. Axonal recording pipette on an 8th order axon branch is illustrated schematically.
(**d**) Plot of latency against distance for $\overline{g_{Na}}$ = 500 pS µm^{-2}. Color scale bar indicates axon branch order (inset, top). Dashed lines indicate the results of linear regression for distances > 100 µm.
(**e**, **f**) Contour plots of reliability (**e**) and velocity (**f**) of AP propagation for the experimentally recorded cell. Note that the reliability of AP propagation is supported above a critical value of $\overline{g_{Na}}$ = 200 pS µm^{-2}, whereas the speed of propagation further increases at supercritical values of $\overline{g_{Na}}$ > 200 pS µm^{-2}. Gray scale bar indicates the value of the indicated parameter (right).

Nature Neuroscience: doi:10.1038/nn.3678

Supplementary Table 1 Density and functional properties of Na^+ channels in BC axons.

Parameter	Axon	Soma
$\overline{g_{Na}}$ [a]	310.7 ± 32.7 pS µm^{-2} (n = 37) 574.3 ± 120.8 pS µm^{-2} (n = 11)	31.9 ± 3.7 pS µm^{-2} (n = 24)
Single Na^+ channel conductance (0 mV) [b]	12.5 ± 1.0 pS (n = 5)	
Open probability Na^+ channels (0 mV) [b]	0.66 ± 0.05 (n = 5)	
Na^+ channel density [a]	25.0 channels µm^{-2} (n = 37) 46.1 channels µm^{-2} (n = 11)	2.6 channels µm^{-2} (n = 24)
Activation time constant (0 mV) [c, d]	64 ± 6 µs (n = 4)	122 ± 34 (n = 9)
Inactivation time constant (0 mV) [c]	303 ± 21 µs (n = 11)	728 ± 98 µs (n = 9)
Midpoint potential activation curve [e]	–42.0 ± 0.7 mV (n = 14)	–31.1 ± 1.3 mV (n = 11)
Slope factor activation curve [e]	7.3 ± 0.5 mV (n = 14)	9.8 ± 0.9 mV (n = 11)
Midpoint potential inactivation curve [e]	–76.6 ± 1.0 mV (n = 13)	–72.1 ± 1.5 mV (n = 6)
Slope factor inactivation curve [e]	8.4 ± 0.6 mV (n = 13)	9.3 ± 1.2 mV (n = 6)
Total surface area of BC axon [f]	40546 µm^2	
Total estimated number of Na^+ channels in BC axon [g]	~1.9 x 10^6	

a Boundary between proximal and distal compartment was set at a distance of 100 µm from axon origin.
b Values determined by nonstationary fluctuation analysis[26,44]; conductance value represents chord conductance.
c For activation and inactivation time constant analysis, only experiments with peak currents > 20 pA were included.
d For measuring activation time constant, only experiments sampled at 100 kHz were included.
e Error estimates were obtained by bootstrap analysis.
f Axonal surface area of BCs according to Nörenberg et al.[9]
g Based on Na^+ channel density in distal axon.

Nature Neuroscience: doi:10.1038/nn.3678